# An Increase in Precipitation Driven by Irrigation over the North China Plain Based on RegCM and WRF Simulations

YUWEN FAN,[a] EUN-SOON IM,[a,b] CHIA-WEI LAN,[c] AND MIN-HUI LO[c]

[a] *Division of Environment and Sustainability, The Hong Kong University of Science and Technology, Hong Kong, China*
[b] *Department of Civil and Environmental Engineering, The Hong Kong University of Science and Technology, Hong Kong, China*
[c] *Department of Atmospheric Sciences, National Taiwan University, Taipei, Taiwan*

(Manuscript received 12 July 2022, in final form 14 March 2023, accepted 18 March 2023)

ABSTRACT: Anthropogenic land-use change, irrigation, is considered to strongly modulate the hydroclimate at the regional scale by directly triggering evaporative cooling as the preliminary local effect. However, subsequent interactions with the background climate are highly nonlinear, which introduces diverse and unexpected consequences. The North China Plain (NCP) is one of the regions where irrigation has expanded the most rapidly since the twentieth century. The scarce rainfall in this region makes it necessary for irrigation to supplement the level of soil water for agricultural production. In this study, we quantify the effect of irrigation on the regional climate in China. Two regional climate models, WRF and RegCM, are used to mimic the large-scale practice of irrigation on the NCP. The results of our experiments show consistent cooling and moistening effects centered over the NCP across all experiments. Although the moisture budget and wind field pattern demonstrate that the vertical downdraft and low-level divergence could inhibit rainfall, the humidification dominates the climatic response in the dry April–June and increases the amount of precipitation significantly and consistently in the NCP region and the surrounding area in northern China. The enhanced CAPE increases sharply on some "calm days" when the vertical moisture advection is small, especially during the afternoon, triggering frequent light rains convectively by destabilizing the atmosphere. The consistent response to irrigation in two different models that employ structurally different land surface schemes could enhance the robustness of the physical mechanism behind the precipitation increase in the heavily irrigated region of NCP.

KEYWORDS: Atmosphere-land interaction; Hydrometeorology; Climate models

## 1. Introduction

As an effective solution to guarantee the water demand in productive cultivation (Foley et al. 2011), irrigated agriculture accounts for roughly 40% of total world cereal production (Bonfils and Lobell 2007). With its substantial expansion since the twentieth century, irrigation is now responsible for over 70% of global freshwater withdrawals (Siebert et al. 2010). Unsurprisingly, therefore, this intensive and extensive irrigation has attracted considerable attention from scientists and the general public alike, especially against the current background of climate change.

Compared with rain-fed agriculture, irrigation adds extra water into the system, and alters the land surface conditions by increasing the soil moisture and fraction of green vegetation (Wu et al. 2018). On a local scale, wet soil facilitates evaporation and vigorous plant growth enhances transpiration, both of which generate relatively more latent heat in irrigated areas, as well as a surface cooling effect during the growing season, which is considered the first-order effect of irrigation (Cook et al. 2011; Segal et al. 1998). Moreover, the elevated levels of water vapor derived from the associated evapotranspiration lead to potential variations in radiative forcing and water cycling (Gordon et al. 2005; Wada et al. 2017; Yang et al. 2019). The enhanced water vapor and latent heat may facilitate moisture condensation and upward air movement that have the tendency to trigger precipitation (Boucher et al. 2004). On the other hand, the surface sensible heat flux is curtailed owing to energy repartition (Pokhrel et al. 2012) and the primary cooling effect may stabilize the atmosphere, both of which inhibit convection locally (Pei et al. 2016). These contradicting forces shape an unpredictable precipitation response to irrigation that depends greatly on the local prerequisite conditions for rainfall formation. Moreover, other climatic processes such as cloud formation, local circulation, moisture transport and so on, are probably affected implicitly, and these changes may exert further influence on the local climate during the irrigation season (Boucher et al. 2004; Huber et al. 2014). Furthermore, a few studies have implied that the irrigation impact can extend temporally and spatially, for instance by exerting a warming effect in boreal winter in midlatitude and tropical regions in the Northern Hemisphere and altering the scale of circulation in the planetary boundary layer to affect the continental climate (Puma and Cook 2010; Lee et al. 2011).

The climatic impact of irrigation varies from region to region because of different irrigation extents, local climatology, and land–atmosphere interaction mechanisms (Boucher et al. 2004; Koster et al. 2004; Lobell et al. 2009). Previous assessments analyzed the impact on regional climate using historical

Supplemental information related to this paper is available at the Journals Online website: https://doi.org/10.1175/JHM-D-22-0131.s1.

*Corresponding authors*: Eun-Soon Im, ceim@ust.hk; Min-Hui Lo, minhuilo@ntu.edu.tw

DOI: 10.1175/JHM-D-22-0131.1

observation data and numerical climate models to isolate the irrigation impact from the background climate, especially in regions with particularly intense levels of irrigation. In general, the primary cooling effect of irrigation during the growing season was demonstrated in most major irrigation regions, such as the central United States, eastern China, India, and West Africa, with a significant increase in surface latent heat flux (Im et al. 2014; Tuinenburg et al. 2014; Mueller et al. 2017; Kang and Eltahir 2018). Despite the relative consensus on evaporative cooling, the response to irrigation of local and remote precipitation is more complex because of regional distinctions. For instance, irrigation in India was believed to reduce rainfall by weakening the summer monsoon (Puma and Cook 2010; Tuinenburg et al. 2014) and enhancing the winter monsoon (Wey et al. 2015), and West Africa and Saudi Arabia also saw a consistent reduction in local rainfall over irrigated land, but at the same time a remote increase in precipitation was generated (Im et al. 2014; Lo et al. 2021). The complexity of the situation can also be seen in various studies that have focused on similar study domains. Several researchers suggested that irrigation in the central United States caused higher humidity and weaker Great Plains low-level jet that favor precipitation (Alter et al. 2018; DeAngelis et al. 2010; Yang et al. 2019, 2020). But due to the inhibition of both local convection and large-scale moisture convergence, the precipitation increase over the irrigated region was also argued to be relatively small, even insignificant compared to its water input (Harding and Snyder 2012a,b; Huber et al. 2014; Qian et al. 2013). Such disagreement on the extent of influence may result from different model settings, since current modeling attempts are still limited in their ability to simulate the effect of irrigation (Leng et al. 2013; Sorooshian et al. 2011).

China is home to 21% of global cereal production in 2019, with the largest agricultural land extent in the world (FAO 2021). More than 40% of the harvested area in China is located on the North China Plain (NCP), and about 41% of the farmland on the NCP is reliant on irrigation. As one of the most intensified agricultural regions in the world, the NCP is characterized by insufficient rainfall and scarce water resources, which greatly enhance the need for irrigation (Zhu et al. 2013). Apart from the region's hydrometeorological background, the distinct thermal contrast between the land and ocean (Lee et al. 2009) also adds complexity to the atmospheric response to irrigation, and there is some debate over the strength of land–atmosphere coupling in China (Koster et al. 2004, 2009; Liu et al. 2014). All these inherent properties of the NCP set it apart from other irrigation hotspots, prompting us to explicate the impacts of irrigation on its regional climate.

Although several global-scale irrigation studies have looked at the impact in northern China with general circulation models (Boucher et al. 2004; Lobell et al. 2009; Puma and Cook 2010; Sacks et al. 2009), regional climate modeling can provide more detailed and region-specific results because of the higher spatial resolutions and the better ability to capture spatial variability. For instance, Kang and Eltahir (2019) coupled the Massachusetts Institute of Technology Regional Climate Model, including its irrigation module to the Integrated Biosphere Simulator land surface scheme; Yang et al. (2016) incorporated an irrigation module into the Noah land scheme in the Weather Research and Forecasting (WRF) Model; and Wu et al. (2018) further implemented a more complex irrigation scheme in the Noah-Multiparameterization (Noah-MP) land scheme in WRF that takes the sources of irrigation water and the dynamic feedback of irrigation to vegetation into consideration. Different regional climate models (RCMs) consistently produce the irrigation impact as an overall decreasing temperature and lower planetary boundary layer height (PBLH) near the surface of the NCP and most parts of eastern China (Kang and Eltahir 2019; Wu et al. 2018; Yang et al. 2016), but with distinct precipitation features. More specifically, Kang and Eltahir (2019) suggested that in May–July, irrigation-induced anticyclonic circulation caused by the lower PBLH interacts with the background monsoon and strengthens the low-level moisture convergence along the Taihang Mountains, which significantly increases the precipitation in the NCP region by 20%–40%. However, Yang et al. (2016) and Wu et al. (2018) argued that the stabilization of the cooler atmosphere caused by irrigation counteracts the increasing humidity over the NCP, thereby resulting in heterogeneous changes in summer precipitation; whereas in spring when the atmosphere is relatively stable and dry, the rising moisture overwhelms the cooling effect and thus enhances the precipitation at that time of year. In terms of the remote irrigation impacts, Yang et al. (2016) highlighted increased rainfall in the Yangtze River basin, which borders the south of the NCP, and drier conditions in northern and southern China. Wu et al. (2018) also reported less precipitation in Inner Mongolia and southern China, but the cooling air in the northeast significantly lowers the geopotential height and produces intense cyclones that induce more spring and summer rainfall there. To sum up, there are as yet no firm conclusions or consensus regarding the response of precipitation to irrigation, most likely because of the distinct sensitivities of different RCMs or land schemes.

This study aims to investigate the regional impact of irrigation on precipitation over the NCP and its adjacent area in eastern China by comparing results from two state-of-the-art models: WRF4 and RegCM4. The dynamic crop module in the Noah-MP land scheme and CLM4.5CNCROP module in the Community Land Model (CLM) are activated to realize the application of irrigation based on the soil condition and requirements of plants. To assess the irrigation impact, we conduct a natural experiment (NAT) that simulates natural crop growth without irrigation, and irrigation experiments (IRR) using each climate model. By examining the similarities and distinctions between the different climate models and land schemes, we aim to arrive at some robust conclusions and reveal the potential uncertainty derived from using climate models. Moreover, we also design three sensitivity tests using both WRF and RegCM to simulate the response of the climate to different water forcings, thereby enabling us to ascertain the relationship between the amount of irrigation and the extent of the climatic reaction. Our analysis focuses on identifying the characteristics of spatial precipitation patterns and uncovering which of those patterns of precipitation are more sensitive to the presence or extent of irrigation. Additionally, we assess the dominant factors behind the

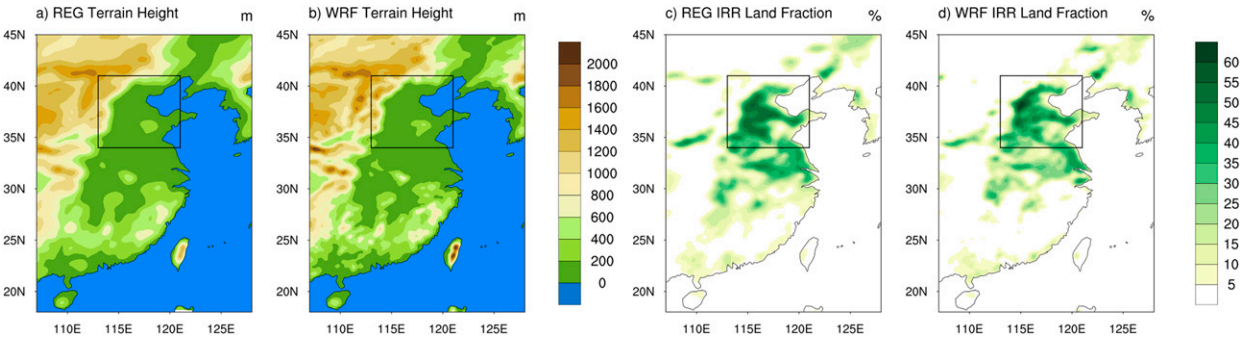


FIG. 1. Model domain showing the (a),(b) terrain height and (c),(d) irrigated land fraction in RegCM and WRF experiments with a horizontal resolution of 25 km (the black box circumscribes the NCP region). Note that the land fraction in (c) will only be used for REGm but not REGs or REGl.

observed precipitation changes by presenting the circulation pattern and instability of the vertical column.

## 2. Model configuration and experimental design

### a. Domain settings

Figure 1 depicts the topography and the fraction of irrigation in our model domain. Following the previous studies (Yang et al. 2016; Kang and Eltahir 2019), the NCP region in this paper is defined as (34°–41°N, 113°–121°E), which includes the most intensified agricultural region in northern China (Figs. 1c,d). As the largest alluvial plain in China (Zheng et al. 2010), the NCP has an average terrain height below 200 m (Figs. 1a,b). To evaluate the regional impact in the NCP and its adjacent area, the whole model domain encompasses the targeted NCP and most of eastern China (18°–45°N, 107°–128°E) with a horizontal resolution of 25 km and 38 vertical layers with 50 hPa as the model top. WRF adopts GMRED2010 (Global Multiresolution Terrain Elevation Data) (Skamarock et al. 2019) for topography, while RegCM adopts GLOBE (Global Land One-km Base Elevation Digital Elevation Model) (Hastings et al. 1999; Oleson et al. 2013), and both of them apply the FAO AQUASTAT database (Global Information System on Water and Agriculture Database of The Food and Agriculture Organization; Portmann et al. 2010; Siebert et al. 2013) as the irrigated land fraction, but different versions. Although their general shapes are similar, RegCM seems to have smoother topography and irrigation fraction under the same resolution as WRF, which is caused by different interpolation methods in the preprocessing. The boundary between the second and third "staircases" of China's topography is clearly outlined by the sharp transition from the plain (in green) to the mountains (in beige).

### b. Experimental design

Since the NAT experiments are designed to simulate the climate without irrigation, irrigation amount should be set to zero, and the irrigation land-use types should be converted to nonirrigation (e.g., rain-fed) cropland, in order to exclude the irrigation impact as much as possible. Then, active irrigation schemes and irrigated plants are incorporated in IRR experiments to estimate the irrigation impact based on historical data in the late twentieth century and early twenty-first century. IRR experiments with small water amounts, moderate water amounts, and large water amounts are conducted using both WRF (WRFs, WRFm, WRFl) and RegCM (REGs, REGm, REGl). WRFm and REGm are designed to be comparable with similar irrigation amounts (Table 1) and irrigated land fractions (Figs. 1c,d). Although moderate water forcing is calibrated according to China's total observed irrigation amount (National Bureau of Statistics of China 2005), the experiment may still overestimate or underestimate the irrigation impact during the simulation processes. To assess the robustness of the results and quantify the uncertainty, sensitivity tests with noticeably smaller and larger water forcings are conducted. Starting from 1 December 1990 and running continuously until the end of February 2011, each experiment

TABLE 1. Abbreviations and irrigation amount of all experiments.

| Experiment | Abbreviation | Irrigation amount ($km^3$ $yr^{-1}$) |
|---|---|---|
| RegCM natural experiment without irrigation | REGn | 0 |
| RegCM irrigation experiment with a small water amount | REGs | 250 |
| RegCM irrigation experiment with a moderate water amount | REGm | 360 |
| RegCM irrigation experiment with a large water amount | REGl | 600 |
| WRF natural experiment without irrigation | WRFn | 0 |
| WRF irrigation experiment with a small water amount | WRFs | 140 |
| WRF irrigation experiment with a moderate water amount | WRFm | 360 |
| WRF irrigation experiment with a large water amount | WRFl | 790 |

covers 20 years with the first 3 months used as spinup (i.e., results between 1 March 1991 and 28 February 2011 are valid).

Comparison of the NAT and IRR experiments will allow us to quantify the irrigation impact on climatic factors, and the results from different models will further assess the reliability and identify the model-related uncertainty. Table 1 lists the abbreviations and the irrigation amount of all the experiments. Due to the data availability, the irrigation is calibrated by country-level data but not grid-based data. This might produce a slight overestimation of the irrigation amount, but the overestimation should be smaller than the difference gap between the sensitivity tests.

For both RegCM and WRF, the initial and lateral boundary conditions are obtained from the ERA Interim Reanalysis released by European Centre for Medium-Range Weather Forecasts, with a resolution of 1.5° × 1.5° and 6-h output intervals, which minimizes the uncertainty arising from the boundary condition (Dee et al. 2011).

### c. *WRF configuration*

As a nonhydrostatic numerical weather prediction model, the Advanced Research version of the WRF Model (version 4.3) is adopted in this study. The main physical options include the WRF double-moment 5-class microphysical parameterization (Hong et al. 2004), the Rapid Radiative Transfer Model as the longwave radiation scheme (Mlawer et al. 1997), the Dudhia shortwave radiation scheme (Dudhia 1989), the Yonsei University planetary boundary layer scheme (Hong et al. 2006), the Kain–Fritsch cumulus parameterization scheme (Kain 2004), and Noah-MP for the initial soil condition as the collocation of the irrigation scheme (Ek et al. 2003).

WRF4.3 (Skamarock et al. 2019) incorporates an irrigation model with Noah as the land surface model (Valmassoi et al. 2020a,b) and another irrigation model with Noah-MP (Niu et al. 2011; He et al. 2023). We adopt the one in Noah-MP since its irrigation is dynamically calculated at each time step based on the soil water deficit, which leans close to the RegCM irrigation scheme, while the Noah one conducts a fixed water amount every day. The irrigation scheme is modified to be applied together with the crop module Liu et al. (2016) only to the grid cells belonging to the crop-related land-use category ("croplands" or "cropland/natural vegetation mosaic") shown in Fig. 1d. Since there will be canopy interception using "sprinkler" and surface loss due to fast "flooding," "drip" is chosen to be applied to all grid cells. It imburses water directly to the soil with the least water loss, which maximizes the utilization rate of water resources, further amplifying the irrigation response. Since irrigation suspension during soil-freezing period is not included in the current scheme, we pause the crop model at the end of November and restart it in the mid-April to exclude the enormous amount of irrigation water in winter and early spring triggered by the dry soil. During the irrigation period, the monthly mean soil temperature in the NCP region is greater than 5°C according to ERA reanalysis data, which is suitable for irrigation (Ozdogan et al. 2010). To maintain consistency with RegCM, the minimum land fraction requirement of irrigation is set to 0.05 (more explanation in section 2d).

Inside the irrigation module, management allowable deficit (MAD) is tuned to apply different water forcings in the simulation. MAD is a decimal number between 0 and 1, representing the level of soil wetness between the wilting status and saturation status. The irrigation module replenishes the soil moisture to this threshold and calculates the water supplement as the irrigation amount if the soil moisture is deficient. Each irrigation ends immediately once the soil moisture reaches the threshold. In the NAT experiment, the irrigation model is turned on but with zero MAD to put no irrigation water, and in WRFm, MAD is set to 0.8 to yield an overall moderate annual water utilization of about 360 $km^3\ yr^{-1}$ compared with the real observation of 380 $km^3\ yr^{-1}$ in 2000 for mainland China (National Bureau of Statistics of China 2005). Besides, sensitivity tests with about half and double of the irrigation amount are also conducted with MAD values equal to 0.7 and 0.9, respectively. Then the crop model calculates the dynamic vegetation growth based on the current soil conditions and agricultural seasons (e.g., planting stage or harvesting stage), leading to more complex climatic responses. Dynamic vegetation for the noncrop region is also turned on to simulate real foliage (Wu et al. 2018).

### d. *RegCM configuration*

To be comparable with the WRF experiment, a nonhydrostatic core is chosen when running RegCM4.7 (Coppola et al. 2021). The domain settings are exactly the same as in the WRF experiment, but the number of vertical layers is set to 23 so as to fit the calculation capability of RegCM. To carry out irrigation scenarios, CLM4.5, with a refined crop model, is used in this study to investigate the irrigation impact (Lawrence et al. 2011; Oleson et al. 2013). Besides, MIT-Emanuel (Emanuel and Živković-Rothman 1999), the subgrid explicit moisture scheme (SUBEX) (Pal et al. 2000), Holtslag (Holtslag and Boville 1993), and the Community Climate Model version 3 (Kiehl et al. 1998) are chosen as the cumulus convection scheme over land and ocean, moisture scheme, the boundary layer physics scheme, and radiation scheme, respectively. These parameterizations are carefully selected based on sensitivity tests over the East Asian domain running a nonhydrostatic core and crop model (Gao et al. 2016; Nguyen-Xuan et al. 2022, 2020).

The interactive irrigation module calculates the daily irrigation at 0600 local time (LT) dynamically according to the soil moisture conditions and crop growth stage (Oleson et al. 2013), which is loosely based on Ozdogan et al. (2010). The irrigation lasts for at most 6 h $day^{-1}$. When the crop model is inactive, all crops are treated as a single land type (i.e., generic crop) and CLM ignores minor land types accounting for less than 19% to avoid processing trivial information. But this curtail of 19% becomes inappropriate after turning on the crop function when a single crop land is classified into eight categories and none of their proportion can reach 19%. Thus, to conduct the irrigation-related experiment, a curtail reduction from 19% to 5% is necessary in order to allow the existence of cropland fractions of more than 5% and to ignore the minor

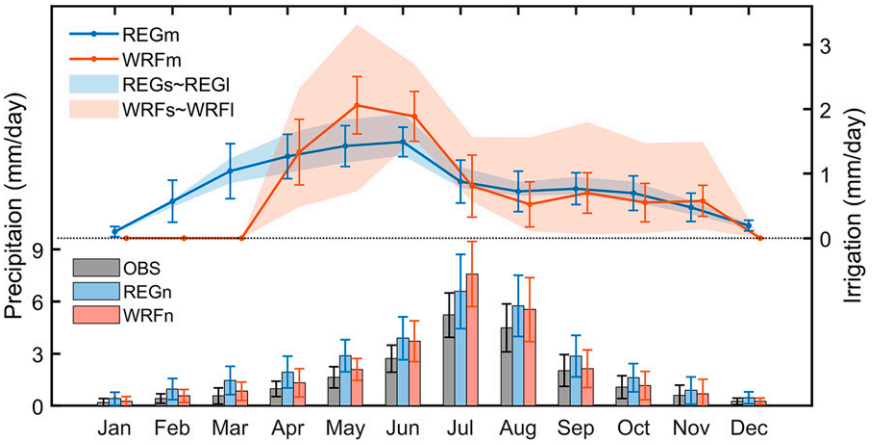


FIG. 2. Monthly precipitation (bars) and irrigation amount (lines) averaged over 20 years. Vertical error bars present the interannual standard deviation of each month. The shading area is bounded by the REGl and WRFl from the top and bounded by REGs and WRFs from the bottom.

land types accounting for less than 5%. The 5% is adopted since the irrigated fractions between REGm and WRFm are more consistent at this curtail. Similar to WRF, the irrigation module in RegCM targets a soil moisture threshold that is defined as a weighted average between minimum soil moisture under no water stress and the maximum soil moisture at saturation state. It depends on the soil texture and the relative proportion of minimum soil moisture which is denoted as irrigation factor (IR). A calibrated IR can establish a more realistic relationship between the irrigated fraction and the water amount. The default IR in the irrigation module in RegCM is calibrated with total world irrigation amount, but it produces overestimation in our domain. Thus, it is essential to recalibrate it again using the statistical data in China. In the REGm, the IR is set to 0.3 to adjust the total simulated water consumption over the target domain to about 370 $km^3\ yr^{-1}$.

Moreover, the irrigation module in the RegCM is only implemented for three of the four irrigated crops (i.e., the irrigation module works for "irrigated corn," "irrigated cereal," and "irrigated soybean," but not "C3 unmanaged irrigated crop") (Oleson et al. 2013). Since the irrigation response depends heavily on the plant reaction (e.g., increased leaf area and evapotranspiration rate after irrigation), all irrigated crops are merged into the corresponding rainfed crop in the natural experiment (REGn). But in REGm, it is necessary to merge the plants in C3 unmanaged irrigated crop into Irrigated Cereal which takes the greatest accounts among the three irrigated crops in the NCP region according to the input data. Otherwise, REGm will contain fewer irrigated crops than WRFm, leading to an unfair comparison between REGm and WRFm. Unlike WRF, the crop phenology determined by the carbon–nitrogen dynamics and crop model (CLM-CNcrop) in RegCM is only growing-stage dependent but not soil moisture dependent. The model prognoses the crop stage based on the recent weather, but the plant distributions are prescribed (Wang et al. 2016). Thus, when conducting the sensitivity tests (REGs, REGl), we directly adjust the irrigated land fraction while maintaining the relationship between land and water unchanged (i.e., IR unchanged). Both C3 unmanaged irrigated crop and C3 unmanaged rainfed crop are combined with irrigated cereal in REGl for those grid cells that already have irrigated crops in REGm, while none of them are modified in REGs. The altered irrigation fractions simulate different vegetation growth under distinct water forcings, leading to different irrigation demands according to the relationship settled in the REGm (Fig. S1 in the online supplemental material). Due to the inflexibility of changing plant types, irrigation differences between REGs and REGl are not as large as that between WRFs and WRFl. But there are noticeable distinctions within the sensitivity tests to clearly identify the correlation between water forcing and irrigation impact in later analysis.

## 3. Results

### a. Validation

Before assessing the irrigation impact, we first compare the model results with observations to prove their predictability. APHRODITE (Yatagai et al. 2012), with comparable resolution to our experiments, is chosen to be the validation data for temperature, while precipitation is compared with the China Meteorological Forcing Dataset (CMFD), with higher resolution. The bar chart in Fig. 2 depicts the annual cycle of the NCP's monthly precipitation in natural simulations. Overestimation of precipitation by REGn seems to systematically exist over the year, while the bias in WRFn is concentrated in the summer when precipitation has higher variability. Although REGn and WRFn overestimate the precipitation amount, both RegCM and WRF still show a reasonable ability in reflecting the temporal variability, especially the pattern of rainy summers (i.e., in July and August). This distinctive surge of summer precipitation in the NCP region, which is widely found in other precipitation data, has a strong correlation with the East Asian

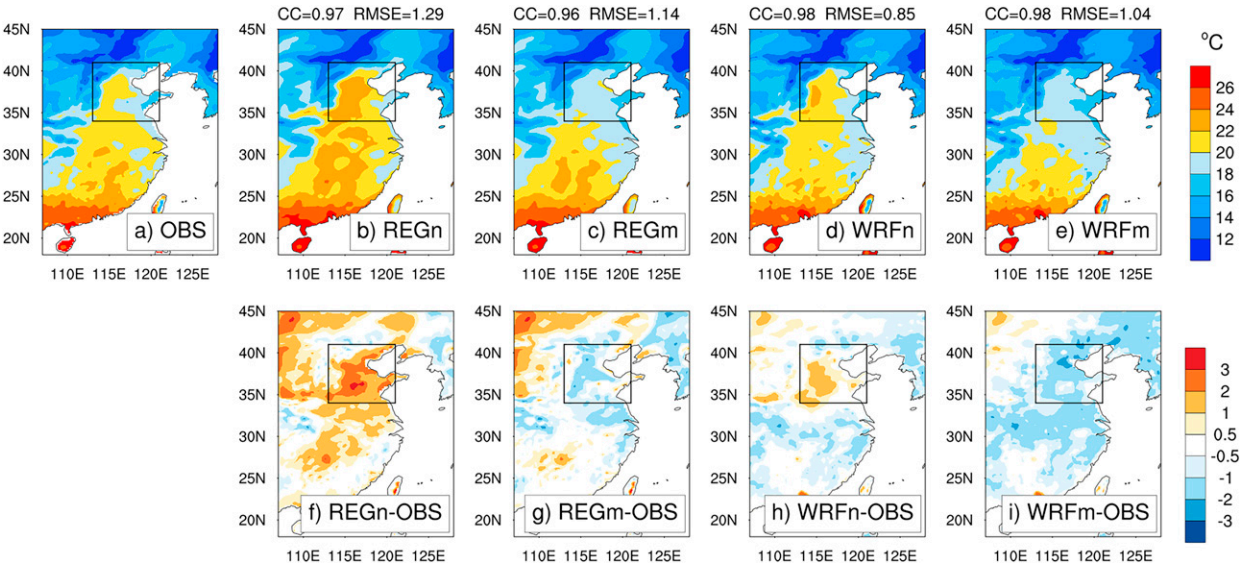


FIG. 3. Spatial distributions of climatological mean temperature (°C) from APHRODITE observations and experiments in AMJ, and their bias. CC stands for correlation coefficient, and RMSE is root-mean-square error.

monsoon (Moiwo and Tao 2015; Sun et al. 2020; Zhang and Lu 2019). The vertical error bars quantify the uncertainty by presenting the interannual standard deviation of each month over the 20-yr period. A similar length of error bars between the observation data and model results validates the models' ability to capture the yearly variation.

Moreover, the lines in Fig. 2 depict the average NCP irrigation amount in each irrigation experiment. The two experiments with moderate water forcing (i.e., the blue and red lines) have comparable annual average irrigation amounts, but REGm performs less temporal variability than WRFm. The smaller distinctions between RegCM sensitivity tests than the WRF group can be attributed to fewer differences in total irrigation amount (Table 1). It is reasonable to see that intense irrigation happens in the growing season between April and June. Both WRF and RegCM have a clear response to precipitation replenishment, especially in the wet summer, when irrigation culminates before or in the early summer (i.e., May or June). The presummer irrigation peak has also been found in other irrigation estimation studies, when crop water demand reaches a maximum together with insufficient precipitation (Koch et al. 2020; Wu et al. 2018; Yang et al. 2016). The most significant irrigation impact occurs around May, when the irrigation amount (around 1.5 mm day$^{-1}$) is almost equivalent to half of the monthly precipitation (around 3 mm day$^{-1}$) in April–June (AMJ). Thus, we choose to focus on AMJ when analyzing the irrigation impact, since its substantial water forcings and dry environment give prominence to the irrigation response.

Figures 3 and 4 display spatial comparisons of the mean temperature and precipitation between observations and the natural and irrigation experiments in AMJ. The climatological mean pattern is displayed in the upper row, and then their corresponding bias patterns are in the row below. Irrigation experiments with moderate water forcing are chosen as representatives of all the irrigation experiments. In Figs. 3a–e, temperature shows a gradual decrease from southeast to northwest in eastern China, and this is successfully reproduced by all experiments, with pattern correlation coefficients (CCs) greater than 0.95 and root-mean-square errors (RMSEs) smaller than 1.5°C. WRF performs slightly better than RegCM in capturing the temperature pattern, as indicated by its slightly higher CC and lower RMSE. The natural experiment produces a warm bias especially in REGn, since we modify its default vegetation distribution by merging all irrigated plants to rainfed ones, which slightly reduces its evapotranspiration. The irrigation-induced cooling is already recognizable. Compared with the natural experiments, the irrigation experiments reduce the warm bias over the NCP with both RegCM and WRF, and even generate a cold bias, especially in WRF (Figs. 3f–i). The RegCM performs better in irrigation experiment while WRF performs better in the natural experiment, which is a reflection of the models' default settings. Specifically, WRF is designed to have no irrigation module in the mainstream version (Skamarock et al. 2019), while RegCM comprises several irrigated crops in the vegetation types by default (Oleson et al. 2013). Besides, there is a warm bias at the northwest boundary and to the south of the middle part of the Yangtze River basin in the RegCM experiments, while WRF produces a cold bias at the northeast boundary as well as along the Yangtze River. This can be broadly concluded as a positive temperature bias in RegCM and a negative bias in WRF.

From the precipitation validation results presented in Figs. 4a–e, we can see that all experiments capture the general northward decreasing precipitation pattern, with CCs above 0.75 and RMSEs around or below 2.5 mm day$^{-1}$. Lower RMSEs indicate that RegCM is generally more accurate than WRF, while

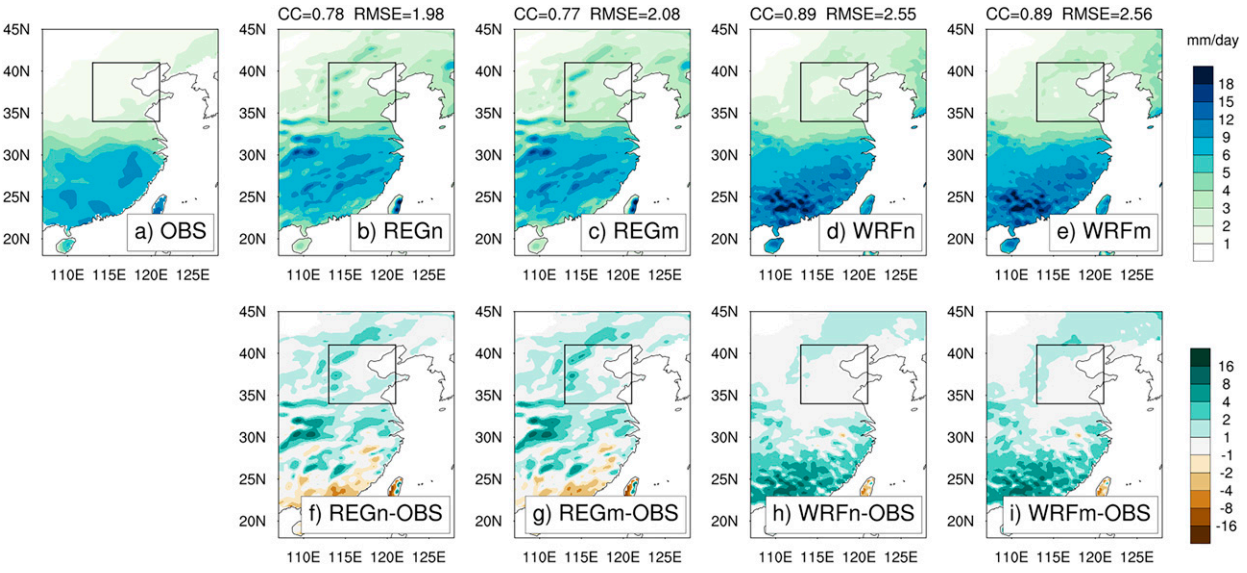


FIG. 4. Spatial distributions of climatological mean precipitation (mm day$^{-1}$) from CMFD observations and experiments in AMJ, as well as their bias.

WRF is better in depicting spatial discrepancy, with a better CC of over 0.9. Different abilities between the two models in reproducing the latitudinal distribution of precipitation are also shown in the bias pattern. WRF generates a wet bias in the southern coastal area, and its wave pattern can probably be attributed to the cumulative impact of gridded land characteristics on convection. RegCM overestimates the precipitation in northern China and underestimates it in southern China, which ultimately leads to a weaker trend but a better balance in overall accuracy. Moreover, both RegCM and WRF generate greater bias along the mountains between the second and third staircases of China's topography. RegCM has a higher sensitivity in the mountainous region, especially around the Qinling and Wushan Mountains near 30°N and 113°E. Indeed, its unsatisfactory performance in the leeward mountainous region has also been reported in other papers (Cheng and Li 2021; Maurya et al. 2020; Verma et al. 2022). However, most of the deviations are consistent within the same model group and can be partially removed by subtraction between the natural and irrigation experiments.

### b. *Irrigation impact comparison between RegCM and WRF*

In this section, we will compare the climatological response to irrigation in AMJ simulated by RegCM and WRF (i.e., REGm and WRFm), which help to understand the model dependencies of water forcing. First, we would like to examine if a similar cooling impact exists, as other studies have proposed. Figure 5 presents the difference in the spatial pattern of the mean irrigation amount, latent heat, PBLH, and near-surface temperature between the moderate irrigation experiments and the natural experiments in AMJ. The pattern of the irrigated regions in Figs. 5a and 5e is highly similar to the irrigation fraction maps in Figs. 1c and 1d. In WRFm, stronger irrigation impact is found in the northern NCP, which is probably caused by the latitudinal transition of soil moisture (Qian and Leung 2007). Due to the sensitivity of RegCM in the area of mountainous terrain, REGm applies excessive water on the leeward side of Taihang Mountain at the western boundary of the NCP's irrigated area. Also, REGm adds less water than WRFm in the northern part of the Yangtze River delta, probably related to its overestimation along the Yangtze River. But, generally speaking, REGm and WRFm produce comparable scales of irrigation.

The increase in latent heat is generally proportional to the water forcing, but in REGm (Fig. 5b), the mountain is not as highlighted as that in the water forcing map (Fig. 5a). This again proves that the overestimation by REGm of the irrigation in the mountainous area can be attributed to its model sensitivity, which should not result in significant deviation in other places. Next, the compression of the PBLH and cooling at the near-surface level are further derived from the increment of latent heat. Compared with WRFm, REGm reacts stronger in terms of PBLH, and also yields a fiercer cooling over the NCP. Both REGm and WRFm experience a greater than 2°C cooling in the central NCP with the land fraction of intense irrigation exceeding 50%, as well as a large-scale effect covering almost the whole domain of eastern China with a temperature drop of less than 0.5°C. Compared with other irrigation studies in the NCP region, the cooling impact reported here is stronger than the responses in spring and summer using smaller or comparable water forcings, because our study focuses only on the most vulnerable month of AMJ (Yang et al. 2016; Wu et al. 2018). But still, our temperature results are weaker than some results using exaggerated water forcings (Kang and Eltahir 2019).

Figure 6 illustrates how irrigation stimulates and transports moisture to form changes in precipitation in AMJ. The spatial

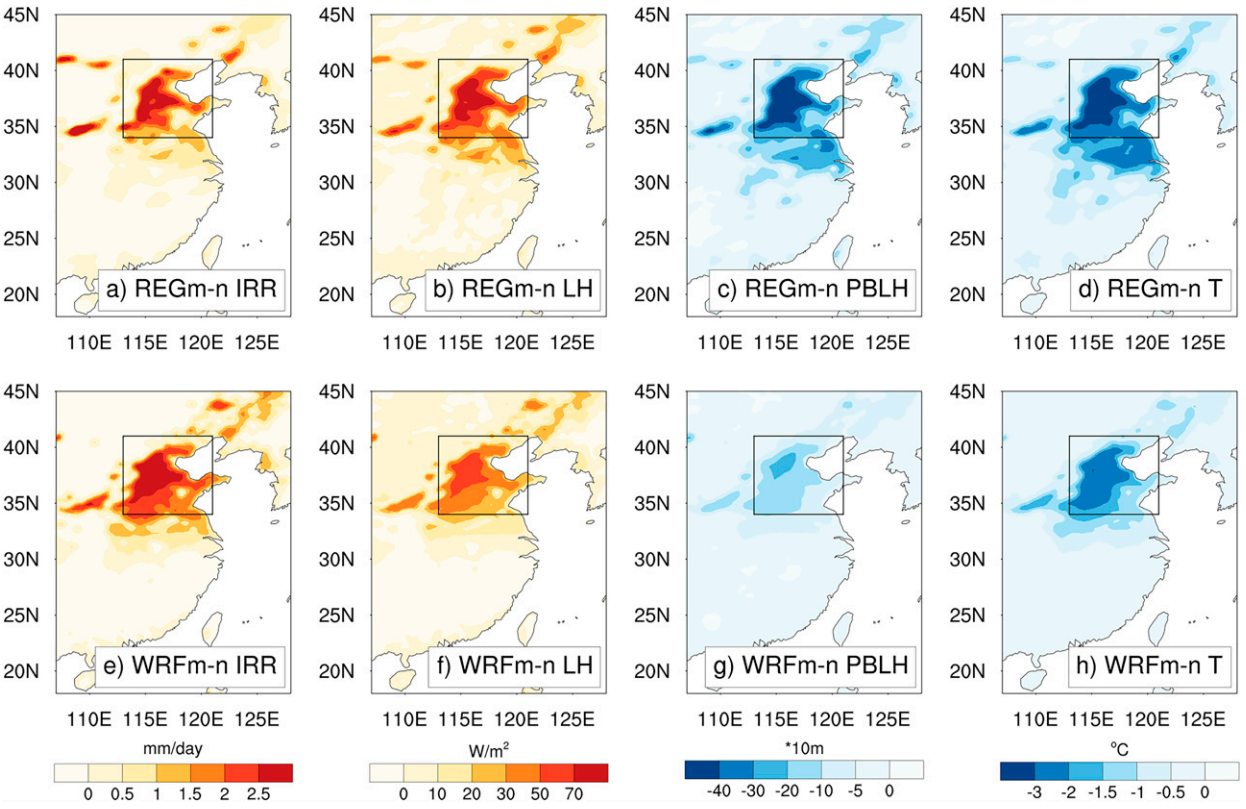


FIG. 5. Spatial distributions of the (a),(e) irrigation amount (mm day$^{-1}$) and irrigation impact on (b),(f) latent heat (W m$^{-2}$), (c),(g) planetary boundary layer height (×10 m), and (d),(h) 2-m temperature (°C), as simulated by (top) REGm and (bottom) WRFm in AMJ.

distribution of relative changes in specific humidity is displayed in cyan color in Figs. 6b and 6f. The greatest humidity change in the NCP region exceeds 30% (i.e., more than 0.000 16 kg kg$^{-1}$) due to its dry background climate, with similar patterns of increased evaporation. Based on this, the total precipitable water over the air column increases in Figs. 6c and 6g, which ensures water availability when the dynamic conditions are suitable for rainfall. Humidity rises in the northern NCP on the leeside of the mountain range are more likely to be retained as precipitable water. The black arrows imposed in Figs. 6b and 6f denote the climatological wind vectors at 850 hPa from the natural experiment, and the moderate-irrigation-induced wind anomalies are indicated by the red arrows. The transport of moisture flux is drawn in a similar way in Figs. 6c and 6g. Similar to other papers (Kang and Eltahir 2019; Im et al. 2014; Lo et al. 2021; Li et al. 2022), irrigation-induced cooling triggers a large-scale clockwise circulation of wind or moisture flux centered over eastern China at low levels and probably stabilizes the atmosphere. The anticyclone drives westerlies in northern China, including the NCP region, the direction of which is the same as the background climate. This wind originates from the arid inland areas of Asia and carries little water vapor (Figs. 6b,f). The water content is replenished as the air passes over the NCP region, and it continues to deliver moisture to northeastern China. In other words, the anomalous westerly flow induced by irrigation intensifies the existing background wind and strengthens moisture transport from the NCP to the northeast, ultimately contributing to a notable humidification in that region. The stronger response in WRF is likely caused by its more concentrated irrigation amount in AMJ.

The humidity increment builds a solid base for precipitation alteration. Figures 6d and 6h only show the precipitation differences in the regions where those differences are statistically significant at the 90% confidence level based on a paired $t$ test of the 20-yr monthly mean in AMJ. These grid cells are considered to have "significant" precipitation changes. Similar to the precipitable water increment in Figs. 6c and 6g, precipitation shows a generally increasing trend in northern China, but a less significant change in southern China in Figs. 6d and 6h. The superimposed dots indicate the areas where the precipitation increases consistently for greater than or equal to 16 years. The statistical testing filters out the ignorable noise and gives prominence to the significant and consistent increases in precipitation in northern China. WRFm simulates a more substantial and expansive precipitation increase that reaches over 0.8 mm day$^{-1}$ and 30%, which matches the magnitude reported in Kang and Eltahir (2019). Although WRFm and REGm have a comparable increase in the near-surface humidity, the precipitation incremental signal in REGm is not as expansive as WRFm, which could be attributed to two reasons. First, it is likely that RegCM itself, especially the MIT-

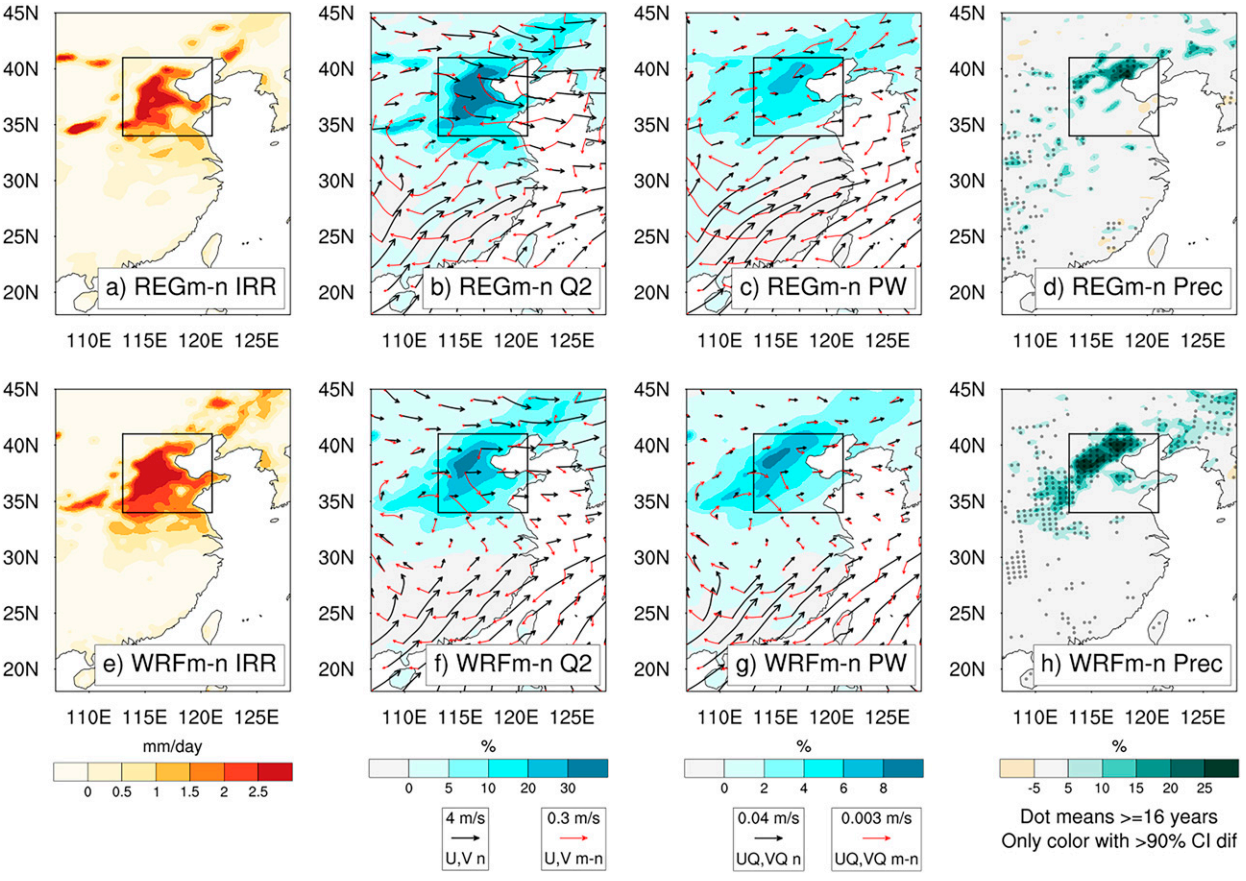


FIG. 6. Spatial distributions of (a),(e) irrigation amount, (b),(f) the relative changes in specific humidity (%) with the 850-hPa wind pattern, (c),(g) relative changes in precipitable water integrated vertically with the 850-hPa moisture flux pattern, and (d),(h) relative changes in precipitation (%), as simulated by (top) REGm and (bottom) WRFm in AMJ. The black arrows in (b), (c), (f), and (g) are the climatological vectors from natural experiments, and the red arrows are the anomaly patterns between the moderate and natural experiments. The superimposed dots in (d) and (h) indicate the areas where a consistent rainfall signal is shown for more than 15 years. The colors in the precipitation-related patterns in (c), (d), (g), and (h) are filtered by 5% changes as well as the two-tailed significance *t* testing at the 90% confidence level.

Emanuel convective scheme, is less sensitive to the humidity increase, leading to less increase in precipitable water and daily rainfall. Second, the overestimation in the NCP precipitation simulated by RegCM may decrease the model sensitivity to additional moisture, which makes RegCM less sensitive than WRF. To assess the dependence of irrigation response on initial conditions, we did another three tests with different initial conditions using RegCM since it contains a weaker signal than WRF (i.e., REGd1, REGd2, and REGd3 are started 1 day, 2 days, and 3 days later than REGm, respectively). Based on Fig. S2, REGd2 and REGd3 perform greater precipitation increase than REGm, while REGd1 has less increase. Generally, they produce highly similar irrigation impacts such as cooling and increasing precipitation, which shows that different initial conditions may not generate significant deviation in our main conclusions. Although REGm has a weaker signal than WRFm, both of them can attain rises of 15% (about +0.3 mm day$^{-1}$), which is comparable to the spring precipitation response reported in Wu et al. (2018).

Figure S3 further shows the irrigation-induced precipitation response in other sensitivity tests. The irrigation amount is presented as lines and shadows on the top (same as Fig. 2), and the monthly average of precipitation increase over the NCP region is presented as bars below. Similar to the irrigation amount, the RegCM experiments have less monthly fluctuation than WRF experiments. The precipitation sensitivity to different water forcings between each sensitivity group can be identified, and both WRF and RegCM contain a positive correlation between irrigation amount and precipitation change most of the months. Although the significant increase only occurs in the northern NCP (Fig. 6), the mean NCP precipitation still rises up to 0.5 mm day$^{-1}$ in May in WRFl. REGl also show an increase of 0.2 mm day$^{-1}$ in April and May. There is a noticeable precipitation decrease around August, but its magnitude is relatively insignificant during the rainy season when the August rainfall is about 6 mm day$^{-1}$ in Fig. 2.

Depicting in a similar way as Figs. 6d and 6h, Fig. 7 shows the decomposed changes in the frequency and intensity of

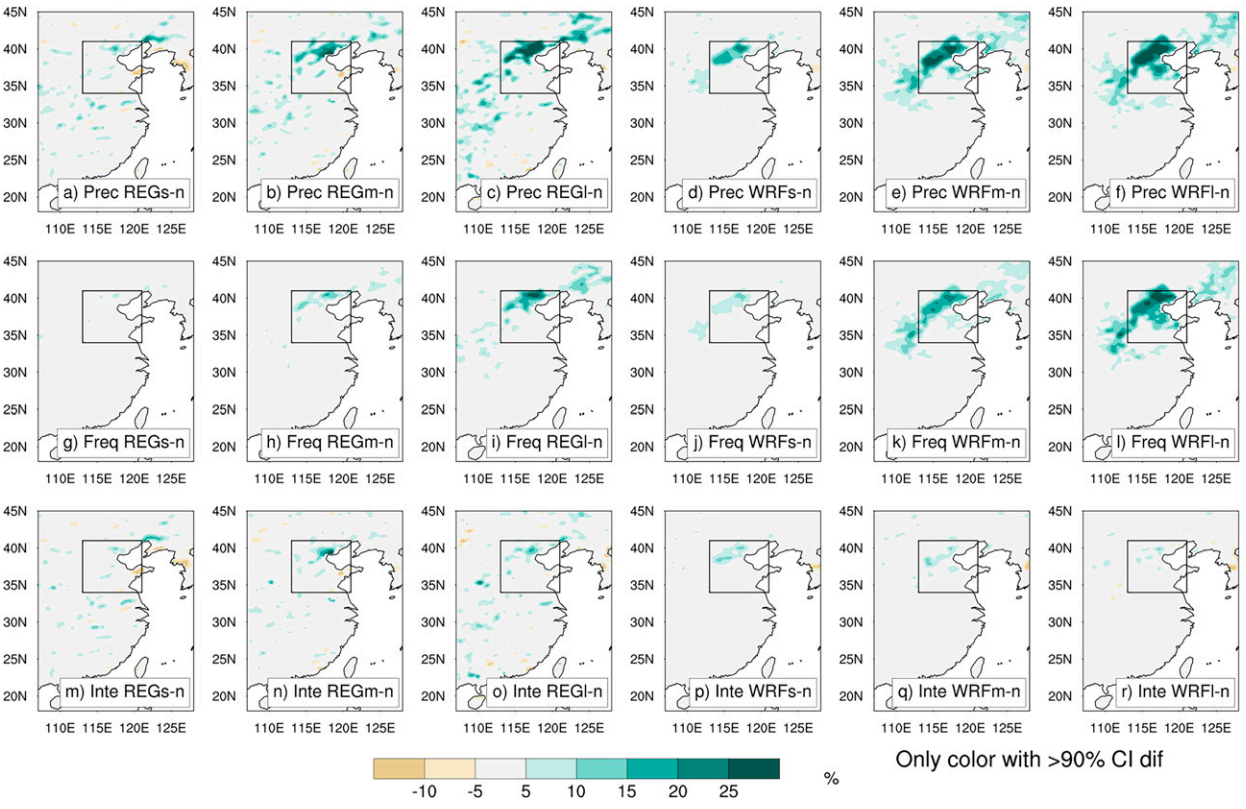


FIG. 7. Spatial patterns of irrigation-induced relative changes in (a)–(f) mean daily precipitation, (g)–(l) rainy days, and (m)–(r) mean daily precipitation on rainy days in AMJ. Only regions with significant precipitation response are presented. A day is classified as rainy when the daily precipitation amount is greater than 1 mm.

rainy days over the whole 20-yr period. A day is classified as rainy if the cumulative daily precipitation exceeds 1 mm, and the intensity is calculated as the average daily precipitation among all rainy days. It is unsurprising to see that the pattern of precipitation change is maintained across the sensitivity experiments in northern China. Also, their magnitudes are proportional to the irrigation water forcing, and the humidification impact seems to extend slightly when the water forcing is enhanced. REGl and WRFl simulate a more substantial signal that can reach 30% (about +0.6 mm day$^{-1}$) of the precipitation increase, which matches the magnitude previously reported in Kang and Eltahir (2019). In areas with significant precipitation changes, including the northern NCP, precipitation frequency plays a more important role than intensity. There are generally more significant increases in the frequency patterns, which should be the principal reason for the precipitation increment in the NCP region in AMJ, while the intensity hardly changed. The dominance of frequency on precipitation response is more prominent with larger water forcings and WRF experiments. This frequency-leading precipitation increase in the NCP region is different from the intensity-leading precipitation increase in the downstream area when irrigation is applied in the central United States in July (Huber et al. 2014).

Figure 8 breaks down the daily precipitation from the viewpoint of convection type. Specifically, grid cells with significant precipitation changes in REGm and WRFm are regarded as the targeted regions that Fig. 8 focuses on. The accumulated bar chart shows the 20-yr average increase in convective and nonconvective precipitation in AMJ over these significant-altered regions. Boxes that are right above the bars indicate their relative increase compared to the natural experiments, while the dots are the relative changes of each year. Generally, the increasing convective rainfall accounts for the main reason for the increment in total precipitation shown by its longer blue bars and higher blue boxes compared with the red ones. The dominance of convective rainfall increase is consistently found in two experimental groups with different convective schemes, but it is more evident with MIT-Emanuel convection scheme in RegCM experiments. A convective precipitation rise of 0.2 mm day$^{-1}$ in REGl can contribute to a more than 40% relative increase. This may imply that the spring atmosphere is overall quite stable and triggers little convection, but after irrigation, convective rainfall increases significantly and consistently with the rising pattern of total precipitation.

### c. *Irrigation impact on convective precipitation*

To understand why convective precipitation is heavily influenced by irrigation, we first pick out the time slot when convective rainfall increases the most during the day since some of the convective activities will not last for the whole day. Only grid cells that have significant precipitation response in

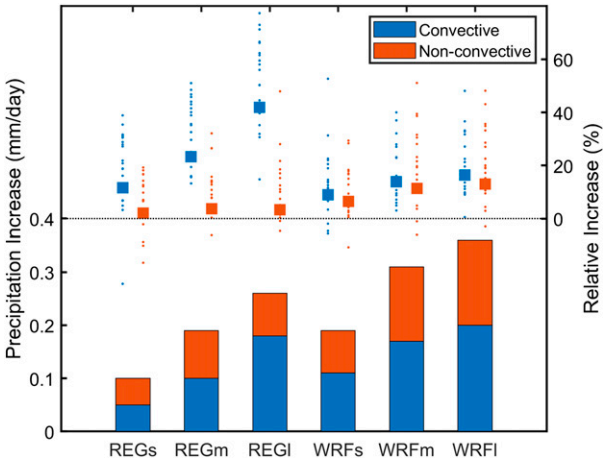


FIG. 8. The regional mean of convective and nonconvective precipitation changes in AMJ is shown by the absolute values (bar chart with *y* axis on the left) and in the percentage form (boxplot with *y* axis on the right). Vertical dots are yearly values, and boxes are the 20 years' climatology mean. Only regions with significant precipitation changes in REGm and WRFm are considered when calculating the regional mean.

REGm and WRFm are colored in Fig. 9. Inside the region with significant rainfall changes in NCP, afternoon convection between 1400 and 2000 LT is most affected by irrigation, which could probably relate to the higher surface temperature during the afternoon. Convection before and after the afternoon (i.e., 0800–1400 LT and 2000–0200 LT) also dominates in a few grid cells, while changes in convective rainfall during the early morning hardly dominate a grid. Since REGm and WRFm irrigate at different times (i.e., REGm irrigates at 0600 LT, WRFm irrigates at any time), the consistency between REGm and WRFm indicates the results should not be heavily dependent on the irrigation time. Thus, we can infer that irrigation promotes afternoon convection, which is the main reason for the precipitation increase in the northern NCP. This is different from the precipitation enhancement mainly induced by nocturnal convection over central United States (Harding and Snyder 2012a; Harding et al. 2015). The inconsistency may come from the distinct background climate since the precipitation mostly happens in the evening and overnight in central United States while peaks in the afternoon in the NCP (Song and Wei 2021).

The appearance of an anticyclonic anomaly in Fig. 6 verifies the existence of a stabilizing effect of irrigation, but it seems to be overwhelmed by the significant moistening effect. To better compare their contributions in a quantifiable way, we analyze the spatial pattern of maximum daily convective available potential energy (CAPE) and convective inhibition (CIN). The climatological values retrieved from the natural experiments are shown in Figs. 10a, 10b, 10e, and 10f, and their changes are displayed in Figs. 10c, 10d, 10g, and 10h. Although both CAPE and CIN increase, the increment of CAPE is more intensive and extensive than that of CIN. In REGm, CAPE increases by more than 50 J $kg^{-1}$, which covers most of the area in NCP and northern China, while CIN increases only by about 20 J $kg^{-1}$ along the leeside of the mountain. Similarly, in WRFm, CAPE rises by even more than 150 J $kg^{-1}$, but CIN only rises by less than 50 J $kg^{-1}$. This predominant increase in CAPE is associated with humidification in the dry atmosphere in the AMJ.

Figure 11 explains why afternoon convection is most affected by displaying the relationship between the enhancement of CAPE and afternoon precipitation using 6-h data during 20-yr AMJ. Averaged value over the NCP region with significant precipitation changes is depicted in the scatterplot. Dots in dark blue represent the time step in the afternoon (1400 LT), while other time steps are in other colors. The dot

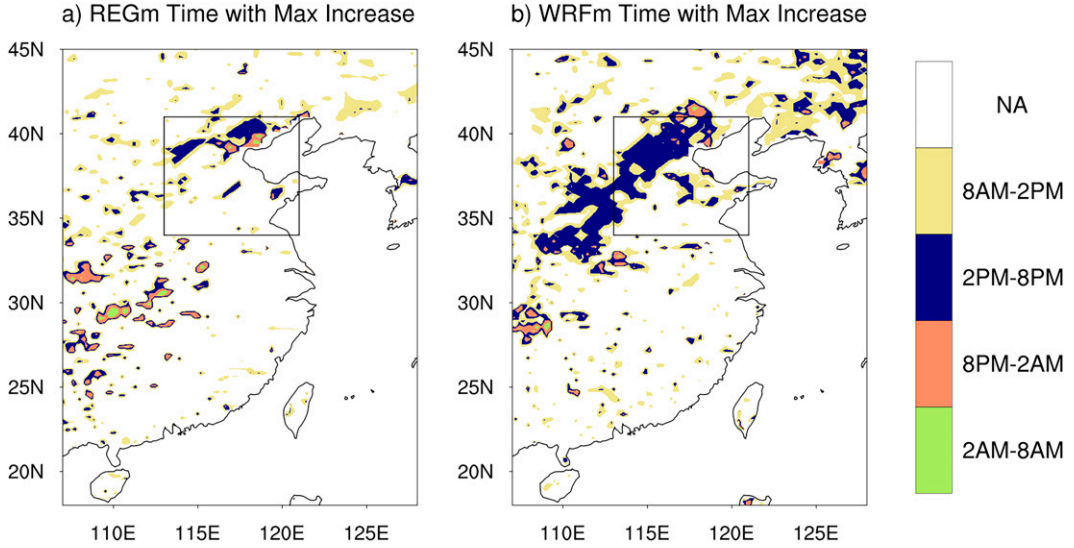


FIG. 9. Time step that triggers the maximum changes in daily convective precipitation in AMJ. Only grid cells that have significant precipitation changes in REGm and WRFm are colored.

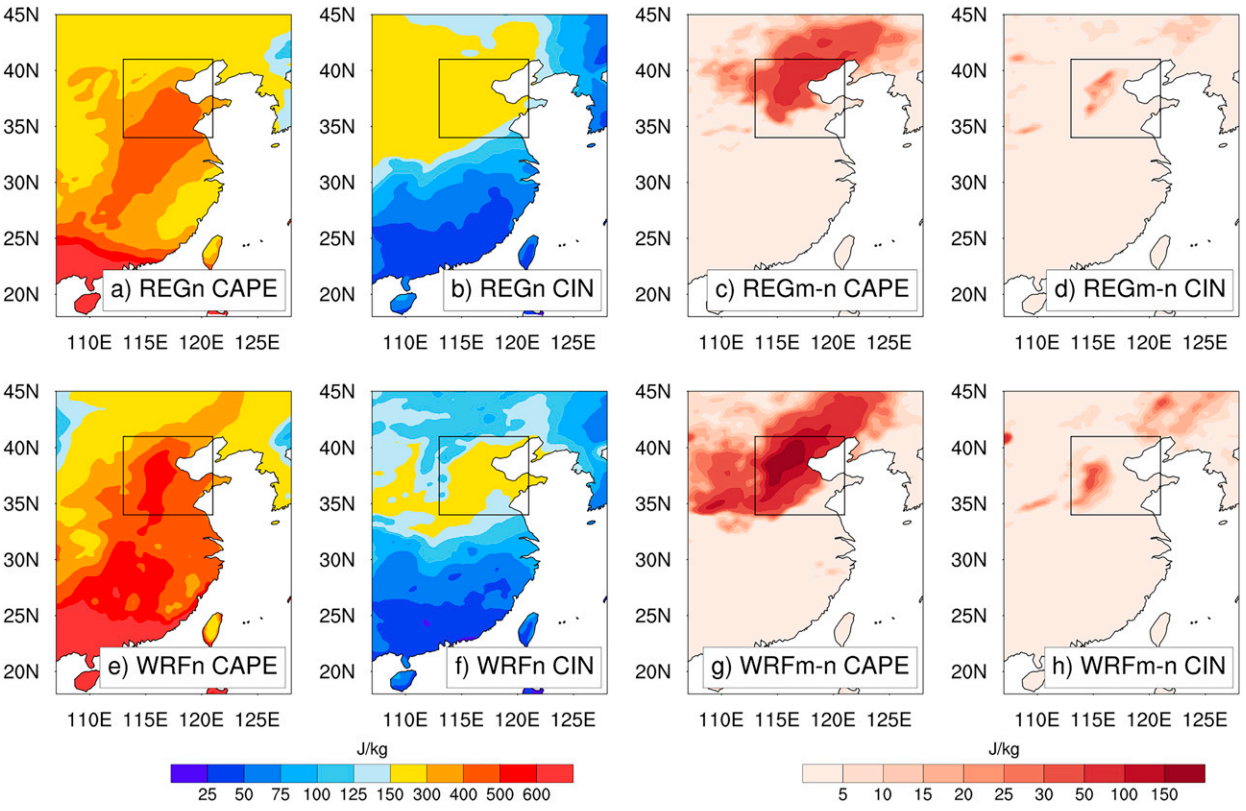


FIG. 10. Spatial patterns of the climatological mean (a),(e) CAPE and (b),(f) CIN calculated from the natural experiment, and the changes in (c),(g) CAPE and (d),(h) CIN caused by irrigation in AMJ as simulated by RegCM4 and WRF.

position in Figs. 11a and 11e is determined by the maximum CAPE and CIN, and the dot size is related to the corresponding precipitation in the natural experiment. During AMJ, afternoon precipitation is relatively heavy, with almost the lowest CIN compared to other time steps. During the afternoon, CIN hardly increases and remains at a low level regardless of the background CAPE or CAPE increase (Figs. 11b,d,f,h), while CAPE keeps increasing with the low CIN (Figs. 11c,g). This finally leads to the sharpest increase in convective rainfall during the day. On the contrary, the slight increase in CAPE in the morning may not produce a substantial impact under the control of its high CIN (i.e., light green color in Figs. 11c,g).

From another perspective, Fig. 12 exposes the vertical structure of precipitation-related variables over the NCP. By using the irrigation-induced changes in afternoon CAPE and CIN integrated from the specific level (denoted as sCAPE and sCIN) (Figs. 12a,d), moist static energy (MSE) (Figs. 12b,e), and dynamic terms of vertical moisture advection (Figs. 12c,f), in which $\omega'$ is the vertical $p$ velocity anomaly and $\overline{q}$ is the climatological mean humidity. As expected from Fig. 10, afternoon CAPE increases much more than afternoon CIN at the midlevel and low level (Figs. 12a,d). The cooling-induced stabilization (blue line in Figs. 12b,e and black line in Figs. 12c,f) dominates the MSE profile (black line in Figs. 12b,e) at around the 700–800-hPa level. But at lower levels, it is overwhelmed by the dramatic increase in latent energy (green line). Finally, driven by the latent moistening, the total MSE (black line in Figs. 12b,e) shifts to a significant positive position. This is consistent with the previous conclusion drawn from the CAPE analysis. The escalation of convective rainfall can be explained by the instability shown by the strong increases in CAPE and MSE, which are conducive to rainfall. However, positive changes in the vertical moisture advection also indicate downward moisture transport that inhibits convective activities, which imposes an opposing impact on precipitation to the increasing CAPE.

The averaged irrigation impact on 6-hourly maximum CAPE and the vertically integrated dynamic term of vertical moisture advection (MADV) over the NCP region are compared in Fig. 13. Figures 13a and 13d indicate how precipitation relates to MADV and CAPE. Large precipitation (large dot) is more likely triggered when MADV is more negative, and drizzle is usually generated under less negative MADV or even positive MADV. Compared with natural experiments (i.e., green dots), more precipitation occurs in the irrigation experiment (i.e., orange dots), especially in the red box where MADV is small and CAPE is large. These newly added dots are dense but generally small, which is consistent with the conclusion from Fig. 7 that irrigation raises the frequency but not the intensity of the precipitation. Figures 13b, 13c, 13e, and 13f are portrayed in a similar way as Figs. 13a and 13d, but without the size difference between dots and their colors

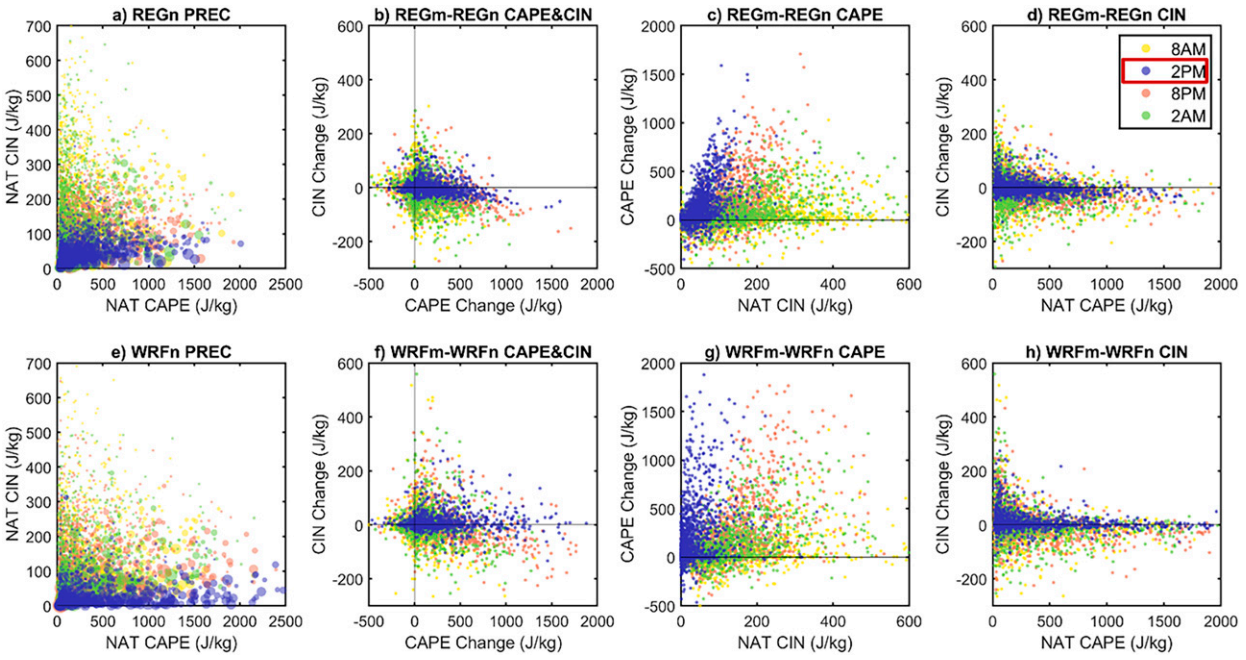


FIG. 11. AMJ 6-hourly (a),(e) maximum CAPE and maximum CIN values in the natural experiment, (b),(f) CAPE and CIN changes from natural to moderate experiment, (c),(g) CAPE change with CIN value in the natural experiment, (d),(h) CIN change with CAPE value in the natural experiment using (top) RegCM and (bottom) WRF. Dots represent the averaged value over those NCP grid cells that have significant precipitation changes in REGm and WRFm. The dot color represents different local times (i.e., yellow is 0800 LT, dark blue is 1400 LT, pink is 2000 LT, and green is 0200 LT) and the dot size in (a) and (e) is related to the 6-h precipitation in the natural experiment.

indicating the CAPE or MADV changes. In Figs. 13b and 13e, the color is gradually deepened along the *x* axis, indicating that the stronger CAPE increase will finally lead to a higher CAPE value in the irrigation experiment. The dots representing the new rainfall inside the red box have greater CAPE increment (in deep blue color). In other words, CAPE increases significantly on calm days when MADV is small, leading to a high CAPE with a small MADV that is more possible to trigger drizzles. According to Fig. S4, whose color indicates the percentage of convective rainfall, convection rainfall accounts for more proportions than nonconvective rainfall in these points. Compared with WRF, convective precipitation is more subordinate in RegCM simulations because almost all the heavy precipitation happening with negative MADV is nonconvective (Fig. S4a). Thus, it would be more difficult to see the blue dots occupy the right tail in REGm (Fig. S4b). On the contrary, convective rainfall happens more frequently in WRFn (Fig. S4c), so most of the new rainfall is generated convectively in WRFm (Fig. S4d). In Figs. 13c and 13f, although MADV increases generally, the colors are more randomly distributed, and there is no significant MADV increase on those dots within the red box. This could also be the reason that CAPE increase can successfully trigger precipitation with little inhibition from MADV.

## 4. Discussion

By conducting regional climate models, local precipitation in the irrigated lands of West Africa, Saudi Arabia, and the central United States shows a general declining or nonsignificant increasing trend of change during the irrigation season, usually the boreal summer. West Africa is controlled by elevated CIN and anticyclonic circulation centered right above the irrigation region, thereby inhibiting both convective and nonconvective rainfall (Im et al. 2014). A similar circulation pattern is found in Saudi Arabia (Lo et al. 2021), probably due to the similar arid climate background in the Middle East and North Africa. In the central United States, moisture divergence is considered to be responsible for the inhabitation on local convection, which undermines the moistening impact and leads to heterogeneous precipitation changes (Harding and Snyder 2012b; Yang et al. 2019). Thus, the significant increase found in the present study may provide some new insights into how irrigation modulates the local precipitation, especially why the moistening impact overwhelms the cooling stabilization and triggers frequent afternoon convection.

Most studies of the irrigation impact in China have focused on the boreal summer season, which keeps a level of consistency with the studies mentioned above. However, our study shows that irrigation culminates before or in the early summer because of the prevailing East Asian monsoon in the mid- to late summer. Although Wu et al. (2018) suggest that the increasing pattern of irrigation in spring is dominated by the moistening over the small downward anomaly, they claimed the existence of a low-level cyclonic anomaly over northeast China, which is different from our results. The circulation pattern in summer is also a matter of debate among different

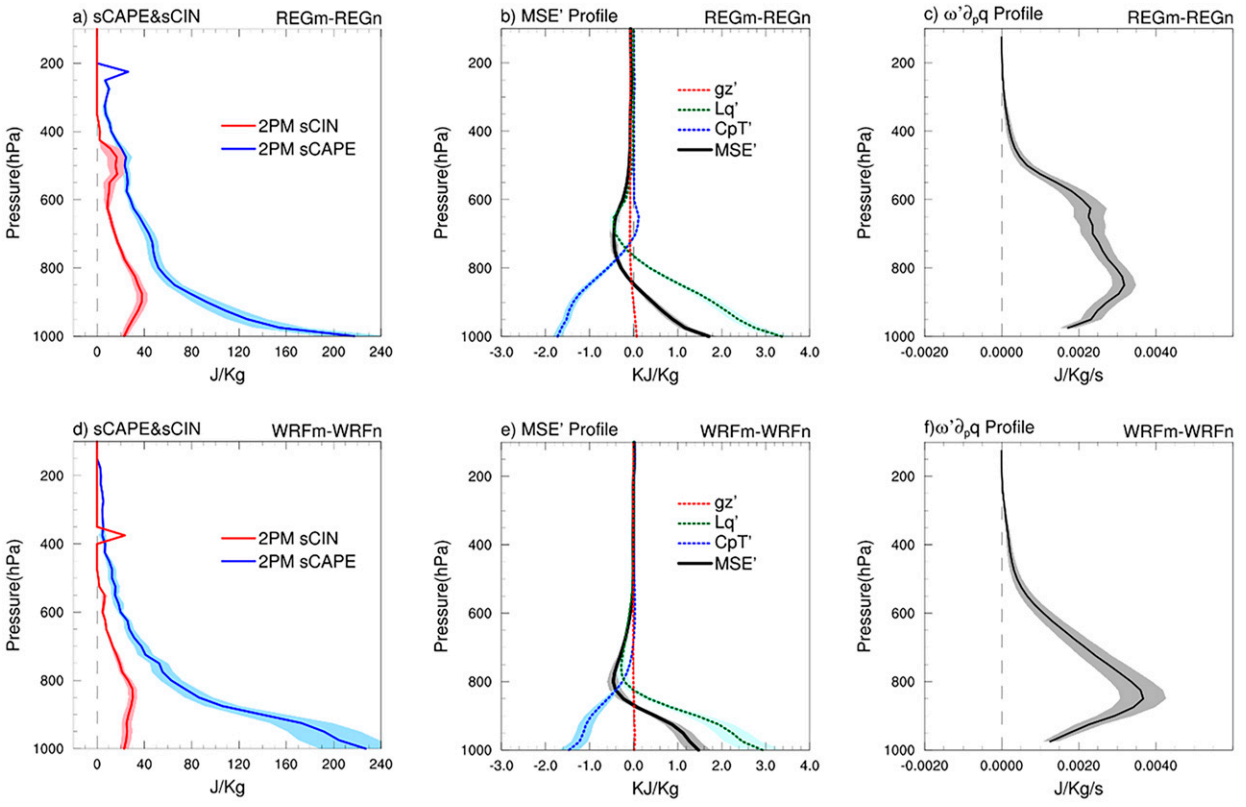


FIG. 12. Vertical profile of difference of (a),(d) sCAPE and sCIN (J $kg^{-1}$) at 1400 LT, (b),(e) MSE (kJ $kg^{-1}$), and (c),(f) dynamic component of vertical moisture advection (J $kg^{-1}$ $s^{-1}$) over land area of NCP. (top) The difference between REGn and REGm; (bottom) the difference between WRFn and WRFm. The shaded area represents the region within 95% confidence intervals for AMJ monthly mean.

studies (Yang et al. 2016; Kang and Eltahir 2019). This inconsistency is likely caused by the unpredictable disruption of the monsoon, since Jeong et al. (2014) stated that the strength of the East Asian summer monsoon can shift and distort the circulation pattern. However, the ambiguity may not falsify our conclusion in AMJ since most precipitation changes are triggered convectively by structural instability. Moreover, we also verify the first hypothesis of agricultural intensification proposed by Alter et al. (2018), that irrigation will generally increase the MSE over cropland areas and enhance precipitation.

One of the main limitations of climate studies is the sensitivity of different climate models and irrigation schemes (Sorooshian et al. 2011; Leng et al. 2013). Our study adopts two different models with distinct land schemes (i.e., Noah-MP and CLM), and draws conclusions on the irrigation impact based only on their consistency. However, this might not fully eliminate the uncertainty derived from climate models. Moreover, there are still notable simplifications and differences in the irrigation behaviors operated by WRF and RegCM4. For example, irrigation is assumed to be conducted once a day in RegCM simulation, and there is no temperature-checking procedure in WRF, which is why we have to manually adjust the irrigation period for WRF to avoid irrigating in the freezing period in winter. These disparities could possibly be solved by localizing the irrigation module to fit the real situation in the NCP region.

This study adopts distinct climate models and convective schemes in WRF and RegCM, but both of them produce overestimated precipitation that can be identified in the temporal (Fig. 2) and spatial patterns (Fig. 4). The wetter soil moisture under the dry background in AMJ may reduce the precipitation sensitivity to extra water induced by irrigation (Kim and Wang 2012). In other words, the irrigation impact on precipitation can probably be weakened by the wet bias generated in REGn, which could be one of the reasons that RegCM shows less significant signals than WRF under comparative water forcings. There are possibilities that the precipitation response would be even stronger if the prediction bias is eliminated. Although WRF contains relatively less bias during AMJ, its overestimation in the southern coastal area could be mitigated by tuning the convective parameters in the Kain–Fritsch scheme, such as extending the CAPE time (Yang et al. 2012, 2015, 2017). The calibration in MIT-Emanuel also has the potential to improve the performance of RegCM by reducing its overestimation of light rains (Zou et al. 2014).

Also, several studies (Wang 2005; Foster et al. 2014; Kang and Eltahir 2018; McDermid et al. 2019) have incorporated other anthropogenic factors, such as greenhouse gas accumulation or groundwater depletion, and put forward incongruent climatic responses such as intensified global warming. Admittedly, irrigation has the potential to produce diverse consequences

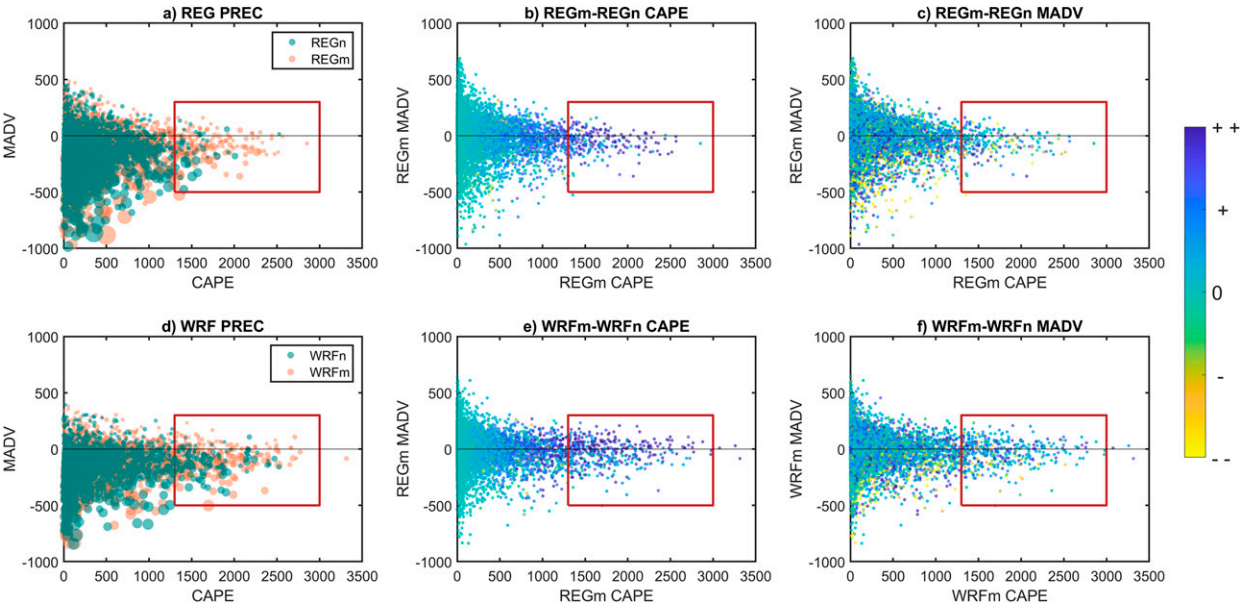


FIG. 13. AMJ 6-hourly (a),(d) CAPE and MADV values in both natural experiment and irrigation experiment. (b),(e) CAPE and MADV values in irrigation experiment colored with CAPE changes. (c),(f) As in (b) and (e), but colored with MADV changes using (top) RegCM and (bottom) WRF. Dots represent the averaged value over all NCP grid cells. Dot sizes in (a) and (d) represent the precipitation rate, and thus, only dots with precipitation greater than 0 will be imposed. In (b), (c), (e), and (f), blue color means an increase, a green color means insignificant change, and a yellow color means a decrease.

under different scenarios because of the nonlinear reactions to it in the climate system.

## 5. Conclusions

This study investigates the impacts of irrigation in the NCP region and its surrounding area, especially on precipitation. To quantify the irrigation impact, 20-yr model experiments are run with and without irrigation using WRF and RegCM. Multiple experiments with different water forcings are conducted as sensitivity tests. Our experiments verify that the most intensive irrigation occurs in late spring or early summer, when there is a large water demand and little precipitation supply. During AMJ, the irrigation-triggered cooling and moistening effect are proportional to the irrigation amount over the NCP. The moistening effect leads to greater latent heat, humidity and more precipitable water in the atmosphere, while cooling drives lower PBL height, large-scale anticyclonic wind differences that cover eastern China, and increase the vertical moisture advection dynamically, which inhibits the formation of precipitation. However, the moistening effect leads to a sharp increase in CAPE especially in the afternoon when CIN is small, resulting in more convective rainfall during the afternoon. On the other hand, CAPE rises significantly on some calm days when the vertical moisture advection is not large enough to prevent rainfall, finally triggering precipitation during more days. Since the small MADV does not favor heavy precipitation, the magnitude of the newly generated rainfall is usually small. MSE analysis also presents the cooling effect is overwhelmed by the humidification in the lower level. Thus, a significant and consistent precipitation increase in the northern NCP is observed in AMJ, and the precipitation increment shows a proportional response to different water forcings in both WRF and RegCM. The summarized flowchart of how irrigation affects the NCP's climate is displayed in Fig. 14.

This study may put forward some new implications on how large-scale irrigation leads to increased precipitation under a particular background climate. Importantly, we draw our conclusions from the results based on the consistency between two state-of-the-art climate models and six sensitivity tests. This greatly improves the reliability of our findings because model and parameterization differences are two of the major

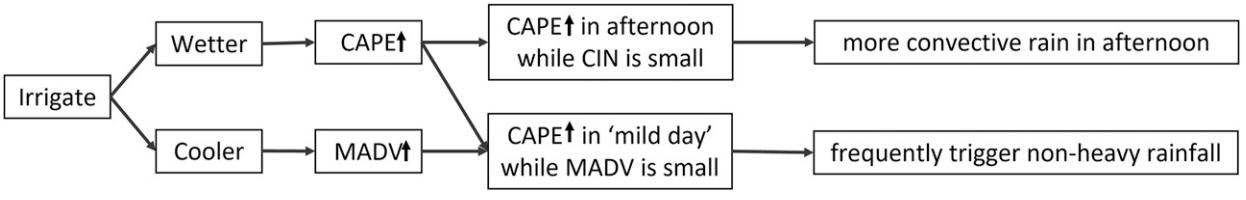


FIG. 14. Schematic diagram of irrigation effects leading to rainfall changes.

uncertainty sources in climate modeling studies. Nonetheless, the differences in irrigation module design and climate models themselves still lead to incongruity in the depiction of summertime precipitation in the NCP region. Further improvement in model design or localization of the parameters may be helpful to generate more practical and consistent results. Overall, our study provides a foundation for future analysis of less model-dependent and more systematic irrigation impacts.

*Acknowledgments.* This study was supported by the Hong Kong Research Grants Council funded project, GRF16309719. The authors thank HKUST Fok Ying Tung Research Institute and National Supercomputing Center in Guangzhou Nansha Sub-center for providing high performance computational resources. The authors declare that the research was conducted in the absence of any commercial or financial relationships that could be construed as a potential conflict of interest.

*Data availability statement.* China Meteorological Forcing Dataset is adopted for the precipitation validation. It is produced by Cold and Arid Regions Science Data Center, Lanzhou, Gansu, China, digital media, doi:10.3972/westdc.002.2014.db. It is available online at http://westdc.westgis.ac.cn.

## REFERENCES

Alter, R. E., H. C. Douglas, J. M. Winter, and E. A. B. Eltahir, 2018: Twentieth century regional climate change during the summer in the central United States attributed to agricultural intensification. *Geophys. Res. Lett.*, **45**, 1586–1594, https://doi.org/10.1002/2017GL075604.

Bonfils, C., and D. Lobell, 2007: Empirical evidence for a recent slowdown in irrigation-induced cooling. *Proc. Natl. Acad. Sci. USA*, **104**, 13 582–13 587, https://doi.org/10.1073/pnas.0700144104.

Boucher, O., G. Myhre, and A. Myhre, 2004: Direct human influence of irrigation on atmospheric water vapour and climate. *Climate Dyn.*, **22**, 597–603, https://doi.org/10.1007/s00382-004-0402-4.

Cheng, Q., and F. Li, 2021: Performance of RegCM4.5 in simulating the regional climate of western Tianshan Mountains in Xinjiang, China. *Atmosphere*, **12**, 1544, https://doi.org/10.3390/atmos12121544.

Cook, B. I., M. J. Puma, and N. Y. Krakauer, 2011: Irrigation induced surface cooling in the context of modern and increased greenhouse gas forcing. *Climate Dyn.*, **37**, 1587–1600, https://doi.org/10.1007/s00382-010-0932-x.

Coppola, E., and Coauthors, 2021: Non-Hydrostatic RegCM4 (RegCM4-NH): Model description and case studies over multiple domains. *Geosci. Model Dev.*, **14**, 7705–7723, https://doi.org/10.5194/gmd-14-7705-2021.

DeAngelis, A., F. Dominguez, Y. Fan, A. Robock, M. D. Kustu, and D. Robinson, 2010: Evidence of enhanced precipitation due to irrigation over the Great Plains of the United States. *J. Geophys. Res.*, **115**, D15115, https://doi.org/10.1029/2010JD013892.

Dee, D. P., and Coauthors, 2011: The ERA-Interim reanalysis: Configuration and performance of the data assimilation system. *Quart. J. Roy. Meteor. Soc.*, **137**, 553–597, https://doi.org/10.1002/qj.828.

Dudhia, J., 1989: Numerical study of convection observed during the Winter Monsoon Experiment using a mesoscale two-dimensional model. *J. Atmos. Sci.*, **46**, 3077–3107, https://doi.org/10.1175/1520-0469(1989)046<3077:NSOCOD>2.0.CO;2.

Ek, M. B., K. E. Mitchell, Y. Lin, E. Rogers, P. Grunmann, V. Koren, G. Gayno, and J. D. Tarpley, 2003: Implementation of Noah land surface model advances in the National Centers for Environmental Prediction operational mesoscale Eta model. *J. Geophys. Res.*, **108**, 8851, https://doi.org/10.1029/2002JD003296.

Emanuel, K. A., and M. Živković-Rothman, 1999: Development and evaluation of a convection scheme for use in climate models. *J. Atmos. Sci.*, **56**, 1766–1782, https://doi.org/10.1175/1520-0469(1999)056<1766:DAEOAC>2.0.CO;2.

FAO, 2021: FAOSTAT database. Accessed 24 December 2021, https://www.fao.org/faostat/en/#compare.

Foley, J. A., and Coauthors, 2011: Solutions for a cultivated planet. *Nature*, **478**, 337–342, https://doi.org/10.1038/nature10452.

Foster, T., N. Brozović, and A. P. Butler, 2014: Modeling irrigation behavior in groundwater systems. *Water Resour. Res.*, **50**, 6370–6389, https://doi.org/10.1002/2014WR015620.

Gao, X.-J., Y. Shi, and F. Giorgi, 2016: Comparison of convective parameterizations in RegCM4 experiments over China with CLM as the land surface model. *Atmos. Oceanic Sci. Lett.*, **9**, 246–254, https://doi.org/10.1080/16742834.2016.1172938.

Gordon, L. J., W. Steffen, B. F. Jonsson, C. Folke, M. Falkenmark, and A. Johannessen, 2005: Human modification of global water vapor flows from the land surface. *Proc. Natl. Acad. Sci. USA*, **102**, 7612–7617, https://doi.org/10.1073/pnas.0500208102.

Harding, K. J., and P. K. Snyder, 2012a: Modeling the atmospheric response to irrigation in the Great Plains. Part I: General impacts on precipitation and the energy budget. *J. Hydrometeor.*, **13**, 1667–1686, https://doi.org/10.1175/JHM-D-11-098.1.

——, and ——, 2012b: Modeling the atmospheric response to irrigation in the Great Plains. Part II: The precipitation of irrigated water and changes in precipitation recycling. *J. Hydrometeor.*, **13**, 1687–1703, https://doi.org/10.1175/JHM-D-11-099.1.

——, T. E. Twine, and Y. Lu, 2015: Effects of dynamic crop growth on the simulated precipitation response to irrigation. *Earth Interact.*, **19**, https://doi.org/10.1175/EI-D-15-0030.1.

Hastings, D. A., and Coauthors, 1999: Global land one-kilometer base elevation (GLOBE) digital elevation model, version 1.0. NOAA National Geophysical Data Center, accessed 25 May 2022, https://www.ngdc.noaa.gov/mgg/topo/globe.html.

He, C., and Coauthors, 2023: The Community Noah-MP Land Surface Modeling System Technical Description Version 5.0. NCAR Tech. Note NCAR/TN-575+STR, 284 pp., https://doi.org/10.5065/ew8g-yr95.

Holtslag, A. A. M., and B. A. Boville, 1993: Local versus nonlocal boundary-layer diffusion in a global climate model. *J. Climate*, **6**, 1825–1842, https://doi.org/10.1175/1520-0442(1993)006<1825:LVNBLD>2.0.CO;2.

Hong, S.-Y., J. Dudhia, and S.-H. Chen, 2004: A revised approach to ice microphysical processes for the bulk parameterization of clouds and precipitation. *Mon. Wea. Rev.*, **132**, 103–120, https://doi.org/10.1175/1520-0493(2004)132<0103:ARATIM>2.0.CO;2.

——, Y. Noh, and J. Dudhia, 2006: A new vertical diffusion package with an explicit treatment of entrainment processes. *Mon. Wea. Rev.*, **134**, 2318–2341, https://doi.org/10.1175/MWR3199.1.

Huber, D. B., D. B. Mechem, and N. A. Brunsell, 2014: The effects of Great Plains irrigation on the surface energy balance,

regional circulation, and precipitation. *Climate*, **2**, 103–128, https://doi.org/10.3390/cli2020103.

Im, E.-S., M. P. Marcella, and E. A. B. Eltahir, 2014: Impact of potential large-scale irrigation on the West African monsoon and its dependence on location of irrigated area. *J. Climate*, **27**, 994–1009, https://doi.org/10.1175/JCLI-D-13-00290.1.

Jeong, S.-J., C.-H. Ho, S. Piao, J. Kim, P. Ciais, Y.-B. Lee, J.-G. Jhun, and S. K. Park, 2014: Effects of double cropping on summer climate of the North China Plain and neighbouring regions. *Nat. Climate Change*, **4**, 615–619, https://doi.org/10.1038/nclimate2266.

Kain, J. S., 2004: The Kain–Fritsch convective parameterization: An update. *J. Appl. Meteor.*, **43**, 170–181, https://doi.org/10.1175/1520-0450(2004)043<0170:TKCPAU>2.0.CO;2.

Kang, S., and E. A. B. Eltahir, 2018: North China Plain threatened by deadly heatwaves due to climate change and irrigation. *Nat. Commun.*, **9**, 2894, https://doi.org/10.1038/s41467-018-05252-y.

——, and ——, 2019: Impact of irrigation on regional climate over eastern China. *Geophys. Res. Lett.*, **46**, 5499–5505, https://doi.org/10.1029/2019GL082396.

Kiehl, J. T., J. J. Hack, G. B. Bonan, B. A. Boville, D. L. Williamson, and P. J. Rasch, 1998: The National Center for Atmospheric Research Community Climate Model: CCM3. *J. Climate*, **11**, 1131–1149, https://doi.org/10.1175/1520-0442(1998)011<1131:TNCFAR>2.0.CO;2.

Kim, Y., and G. Wang, 2012: Soil moisture-vegetation-precipitation feedback over North America: Its sensitivity to soil moisture climatology. *J. Geophys. Res.*, **117**, D18115, https://doi.org/10.1029/2012JD017584.

Koch, J., W. Zhang, G. Martinsen, X. He, and S. Stisen, 2020: Estimating net irrigation across the North China Plain through dual modeling of evapotranspiration. *Water Resour. Res.*, **56**, e2020WR027413, https://doi.org/10.1029/2020WR027413.

Koster, R. D., and Coauthors, 2004: Regions of strong coupling between soil moisture and precipitation. *Science*, **305**, 1138–1140, https://doi.org/10.1126/science.1100217.

——, S. D. Schubert, and M. J. Suarez, 2009: Analyzing the concurrence of meteorological droughts and warm periods, with implications for the determination of evaporative regime. *J. Climate*, **22**, 3331–3341, https://doi.org/10.1175/2008JCLI2718.1.

Lawrence, D. M., and Coauthors, 2011: Parameterization improvements and functional and structural advances in version 4 of the Community Land Model. *J. Adv. Model. Earth Syst.*, **3**, M03001, https://doi.org/10.1029/2011MS00045.

Lee, E., T. N. Chase, B. Rajagopalan, R. G. Barry, T. W. Biggs, and P. J. Lawrence, 2009: Effects of irrigation and vegetation activity on early Indian summer monsoon variability. *Int. J. Climatol.*, **29**, 573–581, https://doi.org/10.1002/joc.1721.

——, W. J. Sacks, T. N. Chase, and J. A. Foley, 2011: Simulated impacts of irrigation on the atmospheric circulation over Asia. *J. Geophys. Res.*, **116**, D08114, https://doi.org/10.1029/2010JD014740.

Leng, G., M. Huang, Q. Tang, W. J. Sacks, H. Lei, and L. R. Leung, 2013: Modeling the effects of irrigation on land surface fluxes and states over the conterminous United States: Sensitivity to input data and model parameters. *J. Geophys. Res. Atmos.*, **118**, 9789–9803, https://doi.org/10.1002/jgrd.50792.

Li, J., Y. Qian, L. R. Leung, Z. Feng, C. Sarangi, Y. Liu, and Z. Yang, 2022: Impacts of large-scale urbanization and irrigation on summer precipitation in the mid-Atlantic region of the United States. *Geophys. Res. Lett.*, **49**, e2022GL097845, https://doi.org/10.1029/2022GL097845.

Liu, D., G. Wang, R. Mei, Z. Yu, and H. Gu, 2014: Diagnosing the strength of land–atmosphere coupling at subseasonal to seasonal time scales in Asia. *J. Hydrometeor.*, **15**, 320–339, https://doi.org/10.1175/JHM-D-13-0104.1.

Liu, X., F. Chen, M. Barlage, G. Zhou, and D. Niyogi, 2016: Noah-MP-Crop: Introducing dynamic crop growth in the Noah-MP land surface model. *J. Geophys. Res. Atmos.*, **121**, 13 953–13 972, https://doi.org/10.1002/2016JD025597.

Lo, M.-H., and Coauthors, 2021: Intense agricultural irrigation induced contrasting precipitation changes in Saudi Arabia. *Environ. Res. Lett.*, **16**, 064049, https://doi.org/10.1088/1748-9326/ac002e.

Lobell, D., G. Bala, A. Mirin, T. Phillips, R. Maxwell, and D. Rotman, 2009: Regional differences in the influence of irrigation on climate. *J. Climate*, **22**, 2248–2255, https://doi.org/10.1175/2008JCLI2703.1.

Maurya, R. K. S., M. R. Mohanty, P. Sinha, and U. C. Mohanty, 2020: Performance of hydrostatic and non-hydrostatic dynamical cores in RegCM4.6 for Indian summer monsoon simulation. *Meteor. Appl.*, **27**, e1915, https://doi.org/10.1002/met.1915.

McDermid, S. S., C. Montes, B. I. Cook, M. J. Puma, N. Y. Kiang, and I. Aleinov, 2019: The sensitivity of land–atmosphere coupling to modern agriculture in the northern midlatitudes. *J. Climate*, **32**, 465–484, https://doi.org/10.1175/JCLI-D-17-0799.1.

Mlawer, E. J., S. J. Taubman, P. D. Brown, M. J. Iacono, and S. A. Clough, 1997: Radiative transfer for inhomogeneous atmospheres: RRTM, a validated correlated-k model for the longwave. *J. Geophys. Res.*, **102**, 16 663–16 682, https://doi.org/10.1029/97JD00237.

Moiwo, J. P., and F. Tao, 2015: Contributions of precipitation, irrigation and soil water to evapotranspiration in (semi)-arid regions. *Int. J. Climatol.*, **35**, 1079–1089, https://doi.org/10.1002/joc.4040.

Mueller, N. D., A. Rhines, E. E. Butler, D. K. Ray, S. Siebert, N. M. Holbrook, and P. Huybers, 2017: Global relationships between cropland intensification and summer temperature extremes over the last 50 years. *J. Climate*, **30**, 7505–7528, https://doi.org/10.1175/JCLI-D-17-0096.1.

National Bureau of Statistics of China, 2005: *China Statistical Yearbook*. China Statistics Press, 915 pp.

Nguyen-Xuan, T., L. Qiu, E.-S. Im, J. Hur, and K.-M. Shim, 2020: Sensitivity of summer precipitation over Korea to convective parameterizations in the RegCM4: An updated assessment. *Adv. Meteor.*, **2020**, 1329071, https://doi.org/10.1155/2020/1329071.

——, S. L. Lam, F. Giorgi, E. Coppola, G. Giuliani, X. Gao, and E.-S. Im, 2022: Evaluation of the performance of the non-hydrostatic RegCM4 (RegCM4-NH) over southeastern China. *Climate Dyn.*, **58**, 1419–1437, https://doi.org/10.1007/s00382-021-05969-5.

Niu, G.-Y., and Coauthors, 2011: The community Noah land surface model with multiparameterization options (Noah-MP): 1. Model description and evaluation with local-scale measurements. *J. Geophys. Res.*, **116**, D12109, https://doi.org/10.1029/2010JD015139.

Oleson, K., and Coauthors, 2013: Technical description of version 4.5 of the Community Land Model (CLM). NCAR Tech. Note NCAR/TN-503+STR, 420 pp., https://doi.org/10.5065/D6RR1W7M.

Ozdogan, M., M. Rodell, H. K. Beaudoing, and D. L. Toll, 2010: Simulating the effects of irrigation over the United States in a land surface model based on satellite-derived agricultural

data. *J. Hydrometeor.*, **11**, 171–184, https://doi.org/10.1175/2009JHM1116.1.

Pal, J. S., E. E. Small, and E. A. B. Eltahir, 2000: Simulation of regional-scale water and energy budgets: Representation of subgrid cloud and precipitation processes within RegCM. *J. Geophys. Res.*, **105**, 29 579–29 594, https://doi.org/10.1029/2000JD900415.

Pei, L., N. Moore, S. Zhong, A. D. Kendall, Z. Gao, and D. W. Hyndman, 2016: Effects of irrigation on summer precipitation over the United States. *J. Climate*, **29**, 3541–3558, https://doi.org/10.1175/JCLI-D-15-0337.1.

Pokhrel, Y., N. Hanasaki, S. Koirala, J. Cho, P. J.-F. Yeh, H. Kim, S. Kanae, and T. Oki, 2012: Incorporating anthropogenic water regulation modules into a land surface model. *J. Hydrometeor.*, **13**, 255–269, https://doi.org/10.1175/JHM-D-11-013.1.

Portmann, F. T., S. Siebert, and P. Döll, 2010: MIRCA2000—Global monthly irrigated and rainfed crop areas around the year 2000: A new high-resolution data set for agricultural and hydrological modeling. *Global Biogeochem. Cycles*, **24**, GB1011, https://doi.org/10.1029/2008GB003435.

Puma, M. J., and B. I. Cook, 2010: Effects of irrigation on global climate during the 20th century. *J. Geophys. Res.*, **115**, D16120, https://doi.org/10.1029/2010JD014122.

Qian, Y., and L. R. Leung, 2007: A long-term regional simulation and observations of the hydroclimate in China. *J. Geophys. Res.*, **112**, D14104, https://doi.org/10.1029/2006JD008134.

——, M. Huang, B. Yang, and L. K. Berg, 2013: A modeling study of irrigation effects on surface fluxes and land–air–cloud interactions in the southern Great Plains. *J. Hydrometeor.*, **14**, 700–721, https://doi.org/10.1175/JHM-D-12-0134.1.

Sacks, W. J., B. I. Cook, N. Buenning, S. Levis, and J. H. Helkowski, 2009: Effects of global irrigation on the near-surface climate. *Climate Dyn.*, **33**, 159–175, https://doi.org/10.1007/s00382-008-0445-z.

Segal, M., Z. Pan, R. W. Turner, and E. S. Takle, 1998: On the potential impact of irrigated areas in North America on summer rainfall caused by large-scale systems. *J. Appl. Meteor.*, **37**, 325–331, https://doi.org/10.1175/1520-0450-37.3.325.

Siebert, S., J. Burke, J. M. Faures, K. Frenken, J. Hoogeveen, P. Döll, and F. T. Portmann, 2010: Groundwater use for irrigation—A global inventory. *Hydrol. Earth Syst. Sci.*, **14**, 1863–1880, https://doi.org/10.5194/hess-14-1863-2010.

——, V. Henrich, K. Frenken, and J. Burke, 2013: Global Map of Irrigation Areas version 5. FAO, accessed 27 May 2022, https://www.fao.org/aquastat/en/geospatial-information/global-maps-irrigated-areas/latest-version.

Skamarock, W. C., and Coauthors, 2019: A description of the Advanced Research WRF Model version 4. NCAR Tech. Note NCAR/TN-556+STR, 145 pp., https://doi.org/10.5065/1dfh-6p97.

Song, Y., and J. Wei, 2021: Diurnal cycle of summer precipitation over the North China Plain and associated land–atmosphere interactions: Evaluation of ERA5 and MERRA-2. *Int. J. Climatol.*, **41**, 6031–6046, https://doi.org/10.1002/joc.7166.

Sorooshian, S., J. Li, K.-L. Hsu, and X. Gao, 2011: How significant is the impact of irrigation on the local hydroclimate in California's Central Valley? Comparison of model results with ground and remote-sensing data. *J. Geophys. Res.*, **116**, D06102, https://doi.org/10.1029/2010JD014775.

Sun, J., X. Wang, and S. Shahid, 2020: Precipitation and runoff variation characteristics in typical regions of North China Plain: A case study of Hengshui City. *Theor. Appl. Climatol.*, **142**, 971–985, https://doi.org/10.1007/s00704-020-03344-8.

Tuinenburg, O. A., R. W. A. Hutjes, T. Stacke, A. Wiltshire, and P. Lucas-Picher, 2014: Effects of irrigation in India on the atmospheric water budget. *J. Hydrometeor.*, **15**, 1028–1050, https://doi.org/10.1175/JHM-D-13-078.1.

Valmassoi, A., J. Dudhia, S. Di Sabatino, and F. Pilla, 2020a: Regional climate impacts of irrigation in northern Italy using a high resolution model. *Atmosphere*, **11**, 72, https://doi.org/10.3390/atmos11010072.

——, ——, ——, and ——, 2020b: Evaluation of three new surface irrigation parameterizations in the WRF-ARW v3.8.1 model: The Po Valley (Italy) case study. *Geosci. Model Dev.*, **13**, 3179–3201, https://doi.org/10.5194/gmd-13-3179-2020.

Verma, S., R. Bhatla, N. K. Shahi, and R. K. Mall, 2022: Regional modulating behavior of Indian summer monsoon rainfall in context of spatio-temporal variation of drought and flood events. *Atmos. Res.*, **274**, 106201, https://doi.org/10.1016/j.atmosres.2022.106201.

Wada, Y., and Coauthors, 2017: Human–water interface in hydrological modelling: Current status and future directions. *Hydrol. Earth Syst. Sci.*, **21**, 4169–4193, https://doi.org/10.5194/hess-21-4169-2017.

Wang, G., 2005: Agricultural drought in a future climate: Results from 15 global climate models participating in the IPCC 4th assessment. *Climate Dyn.*, **25**, 739–753, https://doi.org/10.1007/s00382-005-0057-9.

——, M. Yu, J. S. Pal, R. Mei, G. B. Bonan, S. Levis, and P. E. Thornton, 2016: On the development of a coupled regional climate–vegetation model RCM–CLM–CN–DV and its validation in tropical Africa. *Climate Dyn.*, **46**, 515–539, https://doi.org/10.1007/s00382-015-2596-z.

Wey, H.-W., M.-H. Lo, S.-Y. Lee, J.-Y. Yu, and H.-H. Hsu, 2015: Potential impacts of wintertime soil moisture anomalies from agricultural irrigation at low latitudes on regional and global climates. *Geophys. Res. Lett.*, **42**, 8605–8614, https://doi.org/10.1002/2015GL065883.

Wu, L., J. Feng, and W. Miao, 2018: Simulating the impacts of irrigation and dynamic vegetation over the North China Plain on regional climate. *J. Geophys. Res. Atmos.*, **123**, 8017–8034, https://doi.org/10.1029/2017JD027784.

Yang, B., Y. Qian, G. Lin, R. Leung, and Y. Zhang, 2012: Some issues in uncertainty quantification and parameter tuning: A case study of convective parameterization scheme in the WRF regional climate model. *Atmos. Chem. Phys.*, **12**, 2409–2427, https://doi.org/10.5194/acp-12-2409-2012.

——, Y. Zhang, Y. Qian, A. Huang, and H. Yan, 2015: Calibration of a convective parameterization scheme in the WRF model and its impact on the simulation of East Asian summer monsoon precipitation. *Climate Dyn.*, **44**, 1661–1684, https://doi.org/10.1007/s00382-014-2118-4.

——, ——, ——, J. Tang, and D. Liu, 2016: Climatic effects of irrigation over the Huang-Huai-Hai Plain in China simulated by the weather research and forecasting model. *J. Geophys. Res. Atmos.*, **121**, 2246–2264, https://doi.org/10.1002/2015JD023736.

Yang, Z., F. Dominguez, X. Zeng, H. Hu, H. Gupta, and B. Yang, 2017: Impact of irrigation over the California Central Valley on regional climate. *J. Hydrometeor.*, **18**, 1341–1357, https://doi.org/10.1175/JHM-D-16-0158.1.

——, and Coauthors, 2019: Irrigation impact on water and energy cycle during dry years over the United States using convection-permitting WRF and a Dynamical Recycling Model. *J.*

*Geophys. Res. Atmos.*, **124**, 11 220–11 241, https://doi.org/10.1029/2019JD030524.

——, and Coauthors, 2020: Understanding irrigation impacts on low-level jets over the Great Plains. *Climate Dyn.*, **55**, 925–943, https://doi.org/10.1007/s00382-020-05301-7.

Yatagai, A., K. Kamiguchi, O. Arakawa, A. Hamada, N. Yasutomi, and A. Kitoh, 2012: APHRODITE: Constructing a long-term daily gridded precipitation dataset for Asia based on a dense network of rain gauges. *Bull. Amer. Meteor. Soc.*, **93**, 1401–1415, https://doi.org/10.1175/BAMS-D-11-00122.1.

Zhang, Z., and C. Lu, 2019: Spatio-temporal pattern change of winter wheat production and its implications in the North China Plain. *Sustainability*, **11**, 3028, https://doi.org/10.3390/su11113028.

Zheng, C., J. Liu, G. Cao, E. Kendy, H. Wang, and Y. Jia, 2010: Can China cope with its water crisis?—Perspectives from the North China Plain. *Ground Water*, **48**, 350–354, https://doi.org/10.1111/j.1745-6584.2010.00695_3.x.

Zhu, X., Y. Li, M. Li, Y. Pan, and P. Shi, 2013: Agricultural irrigation in China. *J. Soil Water Conserv.*, **68**, 147A–154A, https://doi.org/10.2489/jswc.68.6.147A.

Zou, L., Y. Qian, T. Zhou, and B. Yang, 2014: Parameter tuning and calibration of RegCM3 with MIT–Emanuel cumulus parameterization scheme over CORDEX East Asia domain. *J. Climate*, **27**, 7687–7701, https://doi.org/10.1175/JCLI-D-14-00229.1.